



# Thermal behaviour of sulphate-bearing multicomponent silicate–phosphate glasses

Anna Berezicka<sup>1</sup> · Justyna Sułowska<sup>1</sup> · Piotr Jeleń<sup>1</sup> · Radosław Lach<sup>1</sup> · Magdalena Szumera<sup>1</sup>

Received: 28 February 2022 / Accepted: 2 July 2022 / Published online: 1 August 2022  
© The Author(s) 2022

## Abstract

The present study provides a deep insight into the implications of sulphate addition on glass forming properties of materials from the  $\text{SiO}_2\text{--P}_2\text{O}_5\text{--K}_2\text{O--MgO/CaO/MgOCaO}$  systems, by combining: preliminary investigation of as-synthesized materials (XRD, XRF, SEM–EDS), detailed characteristics of their thermal behaviour (DSC), estimation of various glass-stability parameters, in-depth analysis of the course of crystallization and an identification of the crystallized products (XRD, Raman imaging technique). Performed investigations revealed that obtaining amorphous materials is only possible in the system containing MgO as a alkaline earth glass modifier, whereas melts of other tested compositions display high tendency to crystallize during cooling. Thermal investigation showed that the influence of  $\text{SO}_3$  addition on thermal properties of studied materials strongly depends on their composition, but generally such additive increased values of glass transformation temperature and decreased vitreous state transformation range and onset of the crystallization process, compared to the base samples, which is a signal of decrease in thermal stability. Examination of devitrificates revealed the character and distribution of domains present in the structure of studied materials. It was showed that irrespective of composition of the base glass, it is  $\text{K}_2\text{SO}_4$  that precipitates once the sulphate capacity of glass is exceeded and exists in the studied materials as groupings either distributed in the voids of silicate phase, or surrounding the remnants of the gas bubbles embodied within the glass body. The results demonstrated in the present study provide guiding suggestions for development of  $\text{SO}_3$ -containing silicate–phosphate glasses intended especially for applications where release of bioactive ions is sought.

**Keywords** Silicate · Phosphate glasses · Sulphur · Thermal characteristics · Glass transition · Crystallization

## Abbreviations

DSC	Differential scanning calorimetry
$T_g$	Glass transformation temperature
$T_x$	Onset of glass crystallization peak
$T_c$	Maximum of glass crystallization peak
$T_m$	Glass melting temperature

$\Delta H$	Enthalpy of crystallization
$K_A$	Angell parameter
$K_H$	Hruby parameter
$K_T$	Turnbull parameter
$K_W$	Weinberg parameter
$K_{LL}$	Lu and Liu parameter
XRD	X-ray diffraction
XRF	X-ray fluorescence spectroscopy
SEM	Scanning electron microscopy
EDS	Energy-dispersive spectroscopy

✉ Anna Berezicka  
berezicka@agh.edu.pl

Justyna Sułowska  
sulowska@agh.edu.pl

Piotr Jeleń  
pjelen@agh.edu.pl

Radosław Lach  
Radoslaw.Lach@agh.edu.pl

Magdalena Szumera  
mszumera@agh.edu.pl

## Introduction

According to a common theory, any solid substance is able to undergo a vitrification phenomenon and thus adopt an amorphous form, provided that the cooling rate is high enough to prevent crystallization [1].

While such an assumption may be true for the majority of the substances, there exist certain systems for which

<sup>1</sup> Faculty of Materials Science and Ceramics, AGH University of Science and Technology, al. A. Mickiewicza 30, 30-059 Krakow, Poland

acquiring a glassy state is particularly difficult [2]. Such systems consist of elements displaying significant differences in both their chemical properties and the nature of their bonds with the network anions, which limits the possibility to create common bonds between their polyhedra. As proposed by Stoch [2], a formation of the common glass network in those systems will be facilitated by the presence of a component, able to join simultaneously with differing elements through the anion bridges (a ‘buffer’ component). To such systems, one can include the well-known  $\text{SiO}_2\text{--P}_2\text{O}_5$  one, stabilized by the presence of network modifiers (e.g.  $\text{Na}_2\text{O}$ ,  $\text{K}_2\text{O}$ ,  $\text{MgO}$ ,  $\text{CaO}$ ) addition, as well as, much less studied, sulphate-bearing oxide glass systems (silicate, borosilicate, phosphate, among others), as it is known that glass formation in these systems may be facilitated by the alkali/alkaline earth oxides addition [3–6]. In fact, already in 1950 Förland stated that, in order to distort the highly symmetrical  $\text{SO}_4^{2-}$  anion and subsequently facilitate glass formation, it is crucial to combine different cations varying sufficiently in their field strength [7]. Taking the above into consideration, an overall goal of the research that is incorporation of sulphate into the silicate-phosphate glass system has been attempted by in-depth analysis of three distinct compositions of various alkaline earth glass modifiers used ( $\text{MgO}$ ,  $\text{CaO}$ ,  $\text{MgO} + \text{CaO}$ ). The investigation is motivated by the need to develop a glass composition of the most promising sulphate-bearing properties, which in turn would facilitate designing ecological fertilizers in the glassy form, providing plants with bioavailable sulphur as well as other but equally important nutrients such as P, K and Mg.

Glasses of the general  $\text{SiO}_2\text{--P}_2\text{O}_5\text{--K}_2\text{O--MgO--CaO}$  composition are long known as controlled release rate fertilizers and pertain to the group of glass systems in which, when subjected to the action of certain solutions, the process of selective washing-out of their components takes place [8–10]. In the case of such materials, obtaining intended products in the fully amorphous form (e.g. with no crystalline precipitates formed during the processing) is of particular importance from the point of view of their application, i.e. the removal of nutrients into the soil solution. This is related to the fact that the amorphous state, being the state of a higher Gibbs free energy, is usually more soluble than its crystalline counterpart. However, the other consequence of existing in the state of higher energy is an instability of glasses, resulting in the inherent tendency to transform into the more stable crystalline form [11]. And while the process of the growth of crystalline phases might be eligible when used as a strategy to improve the mechanical properties and chemical resistance of glasses (controlled crystallization) [12, 13], an unintended crystallization is highly disadvantageous, as not only adversely affects the biological activity of the abovementioned glasses, but also may lead to unpredictable dissolution rate and mechanism [12, 14]. Therefore,

irrespective of whether one wishes to control crystallization or to avoid it, it is essential to gain detailed knowledge of its course and the tendency of given material to undergo such process.

Unfortunately, obtaining fully amorphous materials in sulphur-bearing glass systems seems to be especially difficult. It is known from the numerous literature data [5, 15–17] that sulphate species, due poor miscibility between silica-rich and sulphur-rich liquids under low pressure conditions, exhibit a poor ability to be incorporated into a silicate-based glass matrix. The amount of  $\text{SO}_4^{2-}$  exceeding the inherent sulphate capacity of a given glass system and hence—not enclosed in the glass network—tends to crystallize either within the matrix or on the glass surface, in the form of sulphate salt phase [5, 16, 18].

It is noteworthy that besides the general reports on the enhanced tendency of  $\text{SO}_3$ -bearing oxide glasses to crystalline sulphate phase formation, literature offers limited data concerning detailed characteristics of their thermal processes. Nonetheless, several studies on the sulphate incorporation into the multicomponent silicate-based glass systems provided some information about the effect of the  $\text{SO}_4^{2-}$  incorporation on the values of glass transformation temperature ( $T_g$ ).

Morizet et al. [19] in his study on anorthite–diopside eutectic (AD) glasses claimed that sulphur dissolved as  $\text{SO}_4^{2-}$  displays only limited or slightly reducing effect on the  $T_g$ . Such results, as contradictory to Morizet’s spectroscopic measurements implying a positive effect of  $\text{SO}_4^{2-}$  groups on the polymerization degree of analysed glasses, were explained by Si–O–S molecular bonds formation. According to the authors, formation of these linkages, apart from being nondetectable by DSC measurements, may mimic the increase in glass polymerization. Similar results were demonstrated by Wu et al. [20], whose research team investigated the influence of  $\text{SO}_3$  addition (0–8 mass%) on properties of barium borosilicate glass–ceramics. Wu’s study revealed that the values of  $T_g$  decreased slightly as more  $\text{SO}_3$  was added to the composition of the analysed materials. Furthermore, the authors found that when the  $\text{SO}_3$  addition content was min. 4 mass% (nominal), barite crystals appear in the bulk of glass–ceramics, but, after an increase in the sulphate load to the nominal value of 8 mass%, a separate sulphate layer was formed on the surface of the sample. It has also been noted by the Wu’s research team that together with increasing  $\text{SO}_3$  addition content, the course of crystallization of studied materials changed from one stage to complex, multistage process. On the other hand, preliminary DTA studies of Manara et al. [5] on  $\text{SiO}_2\text{--B}_2\text{O}_3\text{--Na}_2\text{O}$  ternary glasses showed that, within the investigated composition range, an increase in sulphate content results in a higher  $T_g$ . The authors offered two possible explanations for the observed effect: the first being a hindrance of gliding movements of

the glassy network by sulphate incorporated in the voids of glassy network, while the second was sought in a repolymerization of the silica network as  $\text{Na}^+$  cations are preferably bonded to the sulphate anions. Although an analogous effect of  $\text{SO}_3$  addition on glass transition temperature values was revealed by Lonergan et al. [21], the author emphasized that the difference between the  $T_g$  values observed for the samples with maximum and minimum sulphur loading is minor ( $\sim 20^\circ\text{C}$ ) and therefore exhibits an insignificant effect on glasses' thermal stability. Furthermore, a slowdown in the increase in  $T_g$  values with the  $\text{SO}_3$  content was observed, after the sulphate capacity of the analysed materials reached maximum. The authors postulated that the reason for the observed increase in the studied thermal properties was an increase in the average bond strength for structures of higher dimensionality resulting from the increased cross-linking of the borosilicate framework of the glass.

From the above considerations, it can be clearly seen that the literature data referring to the subject of sulphate influence on the glass transformation process supply different information. Furthermore, it should be stressed that although the value of glass transformation temperature is a quantity of fundamental significance, alone does not provide any direct information on the glass-forming tendency, as it is connected with the chemical composition of glass [22]. Hence, the present study is aimed to thoroughly investigate implications of sulphate addition on glass forming properties of materials from the  $\text{SiO}_2\text{--P}_2\text{O}_5\text{--K}_2\text{O--MgO/CaO/MgO} + \text{CaO}$  systems by combining: detailed characteristics of their thermal processes (glass transition, crystallization and melting), (DSC); estimation of glass-specific parameters, ( $K_H$  [22],  $K_W$  [1],  $K_T$  [23],  $K_A$  [1],  $K_{LL}$  [24]); in-depth analysis of the course of crystallization as well as an identification of the crystallized products (XRD with Rietveld refinement, SEM–EDS, Raman imaging technique). This article provides guiding suggestions for optimizing the production process and defining the composition of sulphur-bearing silicate-phosphate glasses that can fully convert to amorphous state without unintended crystallization, as potential ecological fertilizers supporting plants with bioavailable sulphur.

## Materials and methods

Materials that the present study focuses on are represented by three various compositions  $41\text{SiO}_2\text{--}6\text{P}_2\text{O}_5\text{--}20\text{K}_2\text{O--}33\text{MgO}/33\text{CaO}/16.5\text{MgO} + 16.5\text{CaO--XSO}_3$  (where  $X=0.5, 1, 3$  or  $5$  mol.%), distinguished by the presence of either single alkaline earth oxide (and hence named as MgO series and CaO series) or both those oxides simultaneously (thus designated as MgOCaO series). To test the effect solely of the network modifiers variations on the sulphate solubility in the

designed melts, the contents of all oxide components were kept constant, whereas  $\text{SO}_3$  was introduced in increasing amounts.

Synthesis of glass samples was performed by conventional high-temperature melting of the glass batches. For this purpose, appropriate amounts of high-purity raw materials (i.e.  $\text{SiO}_2$ ,  $(\text{NH}_4)_2\text{HPO}_4$ ,  $\text{K}_2\text{CO}_3$ ,  $\text{MgO}$ ,  $\text{CaCO}_3$  and  $\text{K}_2\text{SO}_4$ ) were mixed in proper quantities in a mortar with a pestle to achieve the desirable homogeneity. Obtained batches were then placed in ceramic crucibles (primarily composed of  $\text{Al}_2\text{O}_3$  and  $\text{SiO}_2$ ), melted in an electrically heated furnace at  $1450^\circ\text{C}$  and then quenched by pouring the melt on a steel plate.

In order to verify the chemical composition of the thus synthesized materials, an X-ray fluorescence spectrometry was applied using an ARL Advant 'XP spectrometer with normalizing glass sample composition to 100%. Values of both nominal and XRF-determined molar contents of individual glass components are presented in Table 1. It should be noted here that the sample nomenclature used in Table 1 and hereafter is organized as follows: the first number gives the nominal  $\text{SO}_3$  molar content, while the letters denote the system under considerations. For example, 0.5S\_CaO sample represents the sample from the CaO series loaded with 0.5 mol.% of  $\text{SO}_3$ .

The scanning electron microscope (SEM) in combination with energy-dispersive spectroscopy (EDS) has been used not only to countercheck the concentrations of oxide components within the studied materials, but also to establish their distribution in the samples' surfaces and to track the visual changes generated by the sulphate addition. For this purpose, observations under high vacuum conditions with a backscatter electron detector (BSE) and an accelerated voltage equal to 18 kV were performed by means of the FEI Nova NanoSEM 200 scanning electron microscope.

Changes in thermal behaviour of obtained samples as a result of introducing increasing amounts of sulphate have been tracked by means of STA 449 F3 Jupiter (NETZSCH) operating in the heat flux DSC mode. Thirty-one milligrams of powder samples having a grain size of 0.1–0.3 mm was heated in platinum crucibles at a rate of  $10^\circ\text{C min}^{-1}$  under the flowing air atmosphere (80 mL min<sup>−1</sup>). As the reference material,  $\text{Al}_2\text{O}_3$  was utilized. For the purpose of establishing characteristic glass parameters, i.e. glass heating process temperatures ( $T_g$ ,  $T_x$ ,  $T_c$ ) and changes of enthalpy of crystallization ( $\Delta H$ ), the Netzsch Proteus Thermal Analysis Program (version 5.0.0.) was applied. The glass transformation temperature ( $T_g$ ) was determined as the mid-point of the corresponding transformation step, while the glass crystallization temperature was derived from the onset ( $T_x$ ) as well as the maximum ( $T_c$ ) of the glass crystallization peak.

The powder X-ray diffraction measurements (PANalytical X-ray Diffractometer X'Pert Pro with Cu lamp in the  $2\theta$

**Table 1** XRF-determined and nominal (in brackets) chemical composition of studied materials [mol.%]

	Sample	SiO <sub>2</sub>	P <sub>2</sub> O <sub>5</sub>	K <sub>2</sub> O	MgO	CaO	SO <sub>3</sub>
MgO-series	0S_MgO	36.58 (41)	6.97 (6)	30.60 (20)	22.38 (33)	–	–
	0.5S_MgO	38.21 (41)	7.19 (6)	25.84 (20)	26.58 (33)	–	0.35 (0.5)
	1S_MgO	35.40 (41)	7.09 (6)	33.13 (20)	20.02 (33)	–	1.04 (1)
	3S_MgO	38.17 (41)	7.08 (6)	27.61 (20)	25.94 (33)	–	2.16 (3)
	5S_MgO	34.67 (41)	6.56 (6)	32.02 (20)	21.70 (33)	–	5.88 (5)
CaO-series	0S_CaO	30.07 (41)	5.04 (6)	19.97 (20)	–	41.01 (33)	–
	0.5S_CaO	31.37 (41)	5.43 (6)	19.73 (20)	–	40.12 (33)	0.58 (0.5)
	1S_CaO	26.06 (41)	4.65 (6)	19.84 (20)	–	46.27 (33)	0.91 (1)
	3S_CaO	32.07 (41)	5.49 (6)	19.58 (20)	–	41.83 (33)	1.91 (3)
	5S_CaO	27.61 (41)	4.80 (6)	20.80 (20)	–	43.04 (33)	5.08 (5)
MgOCaO-series	0S_MgOCaO	29.41 (41)	5.24 (6)	24.01 (20)	8.69 (16.5)	26.53 (16.5)	–
	0.5S_MgOCaO	34.03 (41)	5.90 (6)	22.28 (20)	11.45 (16.5)	22.49 (16.5)	0.57 (0.5)
	1S_MgOCaO	34.63 (41)	6.09 (6)	22.20 (20)	11.88 (16.5)	22.21 (16.5)	0.95 (1)
	3S_MgOCaO	34.56 (41)	6.17 (6)	21.99 (20)	11.99 (16.5)	23.91 (16.5)	2.23 (3)
	5S_MgOCaO	30.63 (41)	5.87 (6)	24.98 (20)	10.75 (16.5)	23.03 (16.5)	8.07 (5)

range 10–70°) were performed not only to verify the amorphous nature of acquired materials, but also to establish the relative content of amorphous and crystalline phases (internal Al<sub>2</sub>O<sub>3</sub> standard method) and to determine the kind of crystalline products in both the as-synthesized materials and the devitrificates.

Preparation of the aforesaid devitrificates comprised of the separation of the fraction containing the 0.1–0.3 mm particles from the synthesized samples and its isothermal heating for 24 h at the crystallization temperatures identified on the basis of the DSC measurements. The nature of the endothermic effect manifesting its presence on the DSC curves of the samples containing 5 mol.% SO<sub>3</sub> has been investigated using X-ray Panalytical Empyrean XRD diffractometer in the range of 10–70° with CuK $\alpha$  radiation. In order to perform the high-temperature studies, Anton Paar HTK 1200 N oven-chamber was used. X-ray diffractograms were recorded between the range of 25–600 °C, whereby the data were collected every 100 °C in the interval of 100–500 °C, every 50 °C in the interval of 550–600 °C and additionally at the temperature corresponding to the peak maximum (575 °C), both during the heating and the cooling cycle. To record the high-temperature diffractograms, the sample was first heated at a constant heating rate of 10 °C/min up to the desired temperature, the temperature was held constant for 15 min, and then the data were collected. Next, the same sample was heated again to the subsequent temperature, with the process being repeated for all the temperatures selected.

In order to obtain two dimensions spectral maps of devitrified samples, a confocal Raman imaging system (WITec Alpha 300 M+) equipped with a 488-nm diode laser (laser spot was approx. 650 nm), 1800 grating and a 100×ZEISS Epiplan Neofluar objective. Imaging was conducted in a

40×40  $\mu$ m area, and the scan parameters were as follows: 80 lines with 80points for line. The integration time for a single spectrum was set to 1 s. All mathematical corrections were done using WITec Project Five 5.2 Plus software. In order to establish the chemical composition of the measured surface, a true component analysis was done. Consequently, both maps of component distributions and their spectra were obtained.

## Results and discussion

### Vitrified materials

#### Preliminary evaluation of sulphate-bearing properties of synthesized materials

From the literature data, it follows that the capability of a given glass to incorporate sulphur species is a compositional-dependent feature. Furthermore, as soon as such capability is exceeded, a phenomenon of phase separation takes place, resulting in the formation of crystalline sulphate salt [4, 6, 16, 25]. Therefore, an initial step towards designating the glass composition of the highest potential to incorporate SO<sub>3</sub> constituted a visual inspection of obtained samples complemented with the XRF analysis performed to quantitatively express their sulphate-bearing properties. It is important to mention here that the sulphate-capacity discussed in the present study shall be understood as the maximum SO<sub>3</sub> content, possible to be introduced into the given glass system, without surface crystallization after quenching the melt. Taking the above into account, in Figs. 1, 2, 3 all the obtained samples have been portrayed, together with the

**Fig. 1** Visual and the XRF investigation of the as-synthesized materials from the MgO-series

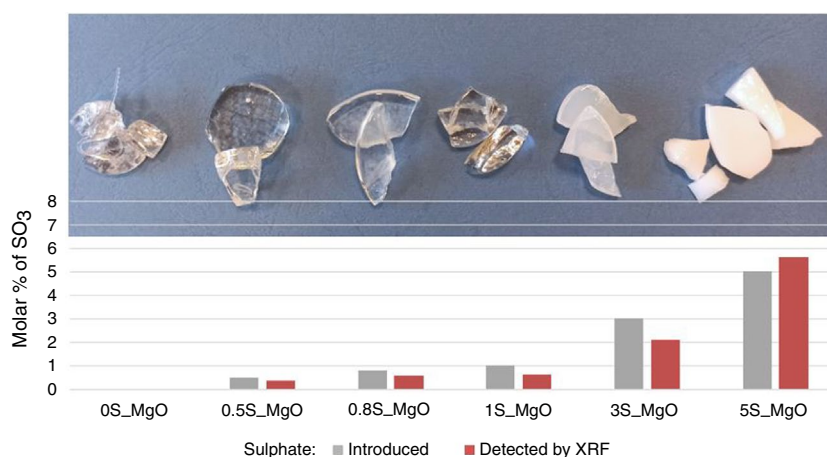


**Fig. 2** Visual and the XRF investigation of the as-synthesized materials from the CaO-series

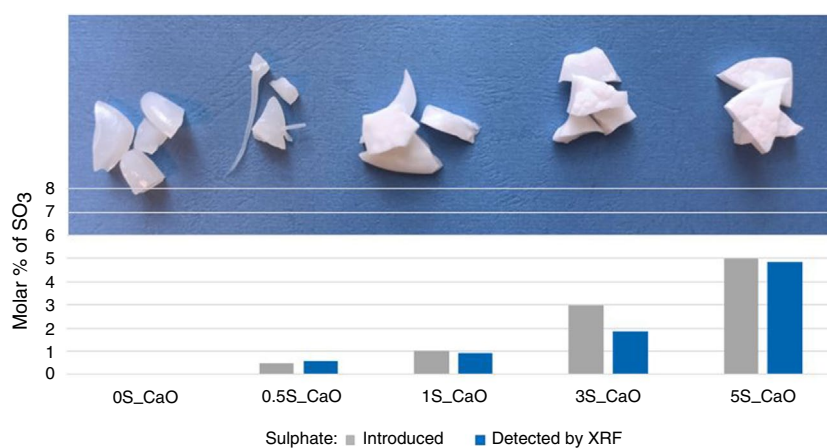
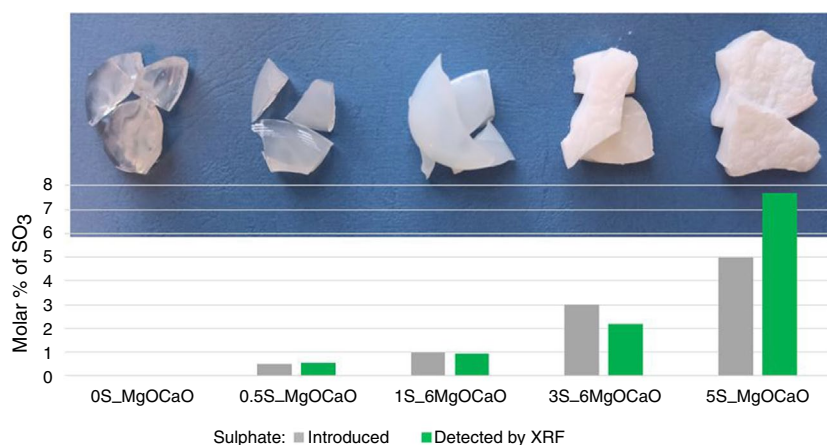


**Fig. 3** Visual and the XRF investigation of the as-synthesized materials from the dual MgOCaO-series



column charts visualizing the XRF-analysed sulphate content of respective materials.

The visual inspection indicated that among all the melt-quenched materials, the only ones exhibiting optical transparency were those from the MgO series (Fig. 1), bearing

0–1 nominal molar content of SO<sub>3</sub>. Beyond this limit of sulphate loading, samples from this very series appeared cloudy (3S\_MgO) or entirely opaque (5S\_MgO). It is known from the previous experience in such kind of materials that opacity of as-synthesized samples is indicative of the process



of spontaneous crystallization, occurring in melts of low viscosity immediately after pouring them onto a steel plate. Meanwhile, as regards the MgO + CaO series notable was the increasing turbidity of the materials representing this system from translucency (0–1 mol.% of SO<sub>3</sub>) towards complete opacity (3, 5 mol.% of SO<sub>3</sub>) (Fig. 1). Similar results were observed in the case of samples constituting the CaO system, except white colouration has been observed already after 1 mol.% of sulphate was introduced into the batch (Fig. 2).

As regards the XRF-based sulphate capacity of studied materials, it appears that the highest potential to incorporate SO<sub>3</sub> displays the MgO series. Such a statement is based on the fact that as much as 2 mol.% of sulphate (i.e. 3 mol.% nominal) has been loaded into this system, until the crystallization (manifesting itself by the complete opacity of the 5S\_MgO sample) took place (Fig. 1). Concurrently, the XRF analysis demonstrated that both the remaining systems (XS\_CaO, XS\_MgOCaO) are able to incorporate ~0.9 mol.% of SO<sub>3</sub> (1 mol.% nominal). Beyond this limit, a white colouration was observed (Figs. 2, 3), implying the formation of crystalline phase, and concomitantly—an exceeded capability of materials to incorporate sulphur. It must also be highlighted that in all samples loaded with 5 mol.% of sulphate, the XRF-analysed sulphate content surpassed (5S\_MgO, 5S\_MgOCaO) or is close to (5S\_CaO) the nominal content (Figs. 1–3). The reasoning behind such a phenomenon may stem from the existence of crystalline sulphate phase nonuniformly distributed in the volume of given materials (presumably on the surface), which in turn distorts the results of XRF analysis, given that, to supplement the foregoing considerations, the SEM–EDS microscopic investigation has been performed, findings of which are presented in the following section.

### Microscopic analysis (SEM–EDS)

The concentrations of SO<sub>3</sub> retained within the samples denoted as: 5S\_MgO, 5S\_CaO as well as 5S\_MgOCaO were counterchecked by the SEM–EDS technique. It was assumed that such an analysis, although only semiquantitative, when performed by averaging the data from several measurement points, would give good approximation of an actual content

of a given component given that the obtained results are tabulated in Table 2, while in Figs. 4–6 the microphotographs together with the EDS spectra are depicted.

From the acquired results, it follows that the molar content of SiO<sub>2</sub>, P<sub>2</sub>O<sub>5</sub>, K<sub>2</sub>O, MgO and CaO in the analysed materials is close to the assumed one (Table 2). This in turn allows one to conclude that the chemical composition of sampling points correspond to the glassy matrix of the investigated samples given that particular attention should be paid to the detected amounts of sulphate and to the substantial difference between those particular results and the XRF-acquired ones as regards all the 5S-samples (see “[Preliminary evaluation of sulphate-bearing properties of synthesized materials](#)” section). Such a discrepancy suggests that the latter results have been affected by the presence of precipitated crystalline sulphate phase. As evidence of the foregoing statement may serve Fig. 6, point 2, demonstrating a region of the 5S\_MgOCaO sample, markedly enriched with sulphur and potassium, and implying at the same time the presence of crystalline K<sub>2</sub>SO<sub>4</sub>. Therefore, it may be stated that for notably crystalline samples, i.e. 5S\_MgO, 5S\_CaO, 5S\_MgOCaO, SEM–EDS-acquired sulphate content (averaged with the exception of the measurement point of the significantly enlarged SO<sub>3</sub> content) mirrors the actual portion of batched SO<sub>3</sub> that has been incorporated into the structure of analysed samples. Meanwhile, the remaining portion of SO<sub>3</sub>, which is the portion that exceeds its sulphate capacity, precipitates as a crystalline phase (judging by the presence of only one such regions observed—presumably in most part located near the surface of studied materials).

It is also informative to explore the development of the microstructure of analysed materials as increasing amounts of sulphate were introduced into their structure. For such a comparison, the MgO series was selected as it is the only system that comprises materials that range from fully transparent, through translucent, to fully opaque. Therefore, Fig. 7 shows the microstructure of the samples: sulphate-free, containing 1 as well as 3 mol.% of SO<sub>3</sub>.

As can be observed in Fig. 7, the examined glasses are free from any crystalline precipitates, and according to the EDS analysis, the chemical composition of the sampling points resembles the assumed one. However, of particular interest are the distinct spherical inclusions in the case of

**Table 2** Semiquantitative concentrations of oxides present in the 5S samples obtained from the SEM–EDS method together with the nominal molar content (in brackets). Additionally, the XRF-determined SO<sub>3</sub> content has been presented for comparison (SO<sub>3</sub> {XRF})

No	SiO <sub>2</sub>	P <sub>2</sub> O <sub>5</sub>	K <sub>2</sub> O	MgO	CaO	SO <sub>3</sub>	SO <sub>3</sub> {XRF}
5S_MgO	45.4 (41)	7.3 (6)	18.8 (20)	27.3 (33)	–	1.3 (5)	5.88
5S_CaO	36.5 (41)	5.8 (6)	16.9 (20)	–	38.6 (33)	1.6 (5)	5.08
5S_MgOCaO	40.0 (41)	6.3 (6)	19.7 (20)	11.6 (16.5)	21.1 (16.5)	0.9 (5)	8.07

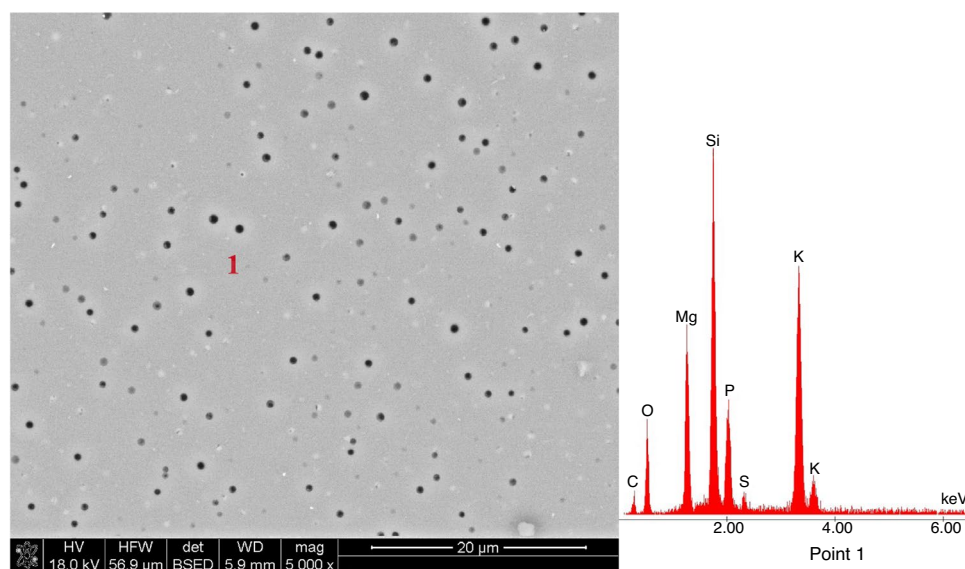


**Fig. 4** SEM microphotograph of the 5S\_MgO sample, together with the EDS spectrum of the glassy matrix

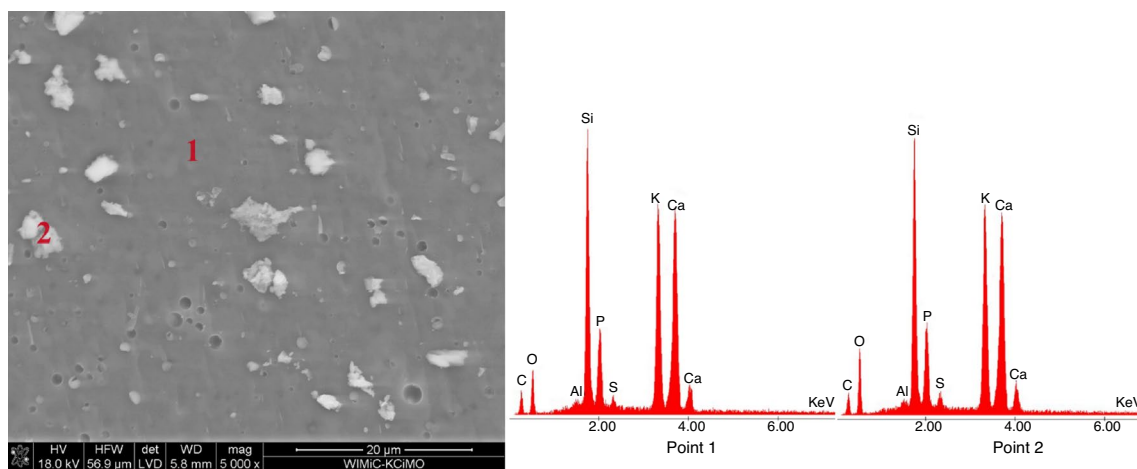


**Fig. 5** SEM microphotograph of the 5S\_CaO sample together with the EDS spectrum of the glassy matrix (point 1,2)

the 3S\_MgO sample, which, although seemingly mysterious, have a straightforward explanation—those peculiarities originate from the gas bubbles developed from the thermal decomposition of batched sulphate. Presumably then, it is the presence of bubbles that contributes to the turbidity of this very sample (Fig. 1, Sect. “[Preliminary evaluation of sulphate-bearing properties of synthesized materials](#)” section).

### X-ray diffraction analysis

To support the preliminary examination of the obtained materials and estimate the relative amounts of the evolved crystalline phases, an XRD method was implemented

together with an internal  $\text{Al}_2\text{O}_3$  standard technique. It should be mentioned here that the procedure of quantitative evaluation of phase content was applied only for samples of suspected crystallinity (i.e. exhibiting translucency/opacity), namely samples containing 3 and 5 mol.% of  $\text{SO}_3$  as regards the MgO series, as well as all the materials representing the remaining systems. Also noteworthy is the fact that the below presented results demonstrating the relative percentage of amorphous and crystalline phases should be considered with caution and treated rather as a general guide, since precise quantification of the fraction of all crystalline phases embodied in the glassy matrix (given the high background of obtained diffractograms) was unattainable using standard XRD technique. Nonetheless, the diffraction patterns together with the identified crystal phases are presented in Figs. 8–10. It should be

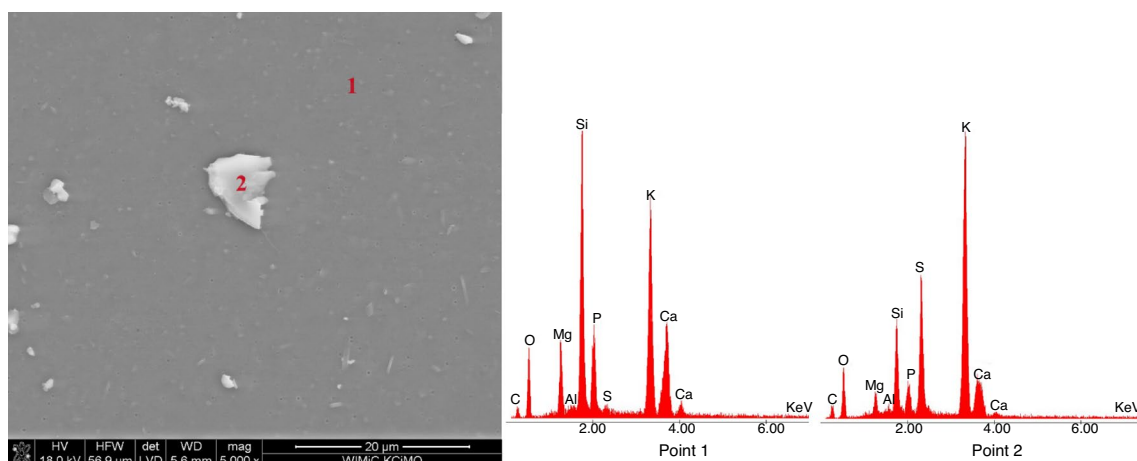


**Fig. 6** SEM microphotograph of the 5S\_MgOCaO sample, together with the EDS spectrum of glassy matrix (point 1) and the sulphur- and potassium-enriched region (point 2)

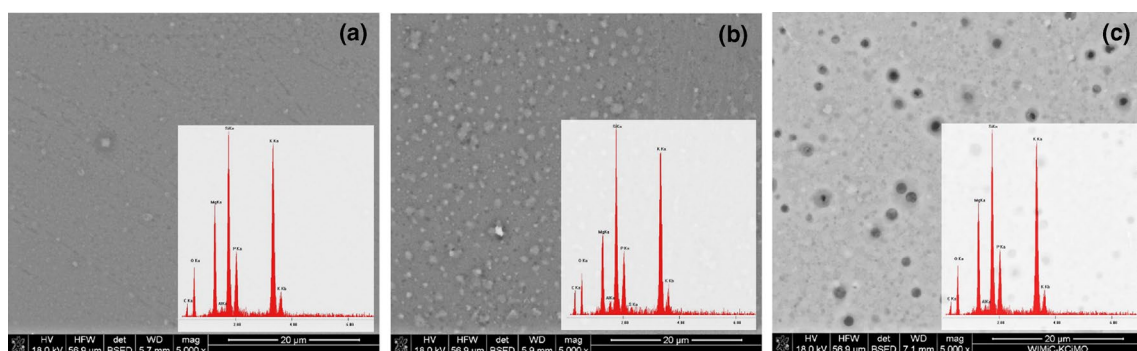


**Fig. 7** SEM microphotograph and EDS spectra of the sulphate-free (a), loaded with 1 (b) and 3 mol.% (c) of SO<sub>3</sub> samples

noted that diffraction peaks originating from the internal standard Al<sub>2</sub>O<sub>3</sub> phase have been marked with blue-coloured line.

Analysis of the XRD patterns of materials representing the MgO series (Fig. 8) revealed the presence of crystalline phase only in the case of the sample containing 5 mol.% of SO<sub>3</sub> (5S\_MgO). The diffractogram acquired for this very material is characterized by low background in relation to the one obtained for the 3S\_MgO sample, as well as intense and well-developed diffraction peaks. In contrast, the glass labelled 3S\_MgO, although visually appeared as cloudy, contains no crystalline phase detectable by the XRD method. As indicated by the phase identification procedure, the only crystalline compound emerging in the MgO system and manifesting itself on the XRD pattern of a glass labelled as 5S\_MgO, is K<sub>2</sub>SO<sub>4</sub> (Fig. 8). Its formation during cooling of the respective sample suggests that the inherent capacity of this very system has been exceeded and therefore—a certain portion of the batched SO<sub>3</sub>, non-incorporated into the glassy matrix, has precipitated as a crystalline sulphate.

Meanwhile, an analysis of the results acquired for the CaO system (Fig. 9) clearly indicated that already in the base sample (i.e. with no sulphate loaded) distinct diffraction peaks are present and overlapped on the relatively high background with a characteristic halo at about 30°. Together with the SO<sub>3</sub> addition, on the XRD patterns of respective samples, one can note a concomitant lowering of the background as well as an increase in the peak intensities. Such an observation may imply an increase in the degree of analysed materials crystallinity along with an increase in sulphate content. This statement is in turn consistent with the findings of the visual examination of the synthesized materials, as the turbidity of the samples increased with the SO<sub>3</sub> addition (see “[Preliminary evaluation of sulphate-bearing properties of synthesized materials](#)” section). Also worth mentioning is the fact that all samples representing the CaO system displayed evident propensity to spontaneous crystallization immediately after pouring the melt onto the plate. Unsurprisingly then, the XRD phase analysis indicated the presence of crystalline compounds in the samples from the CaO



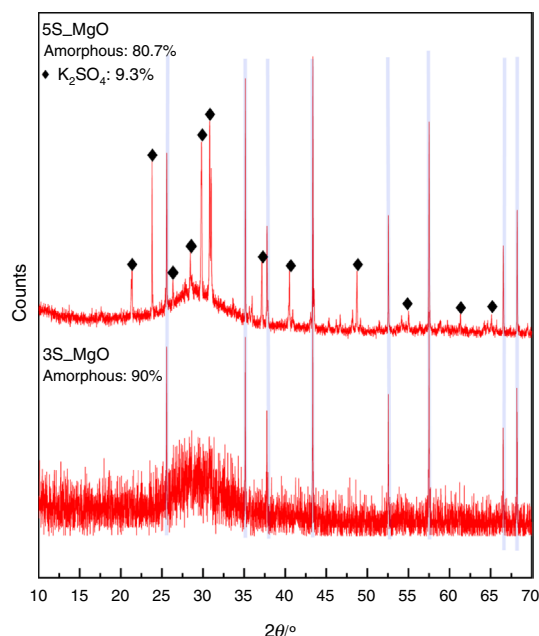


**Fig. 8** X-ray patterns of the samples representing MgO-series, with the assignment of crystalline phases (the amount of corundum used as an internal standard was constant and equal 10 mass%) **Fig. 9** X-ray patterns of the samples representing CaO-series with the assignment of crystalline phases (the amount of corundum used as an internal standard was constant and equal 10 mass%) **Fig. 10** X-ray patterns of the samples representing the MgOCaO-series, with the assignment of crystalline phases (the amount of corundum used as an internal standard was constant and equal 10 mass%)

system, predominantly  $\alpha$ -dicalcium silicate, but also dipotassium sulphate (VI), (Fig. 9). It is valuable to share here the results of multiple studies of Stoch on the crystallization process of silicate–phosphate glasses [2, 26]. According to his research, the succession of crystalline phases formation depends on mobility of the reactants, their concentration and the free enthalpy of compounds synthesis ( $\Delta G_r$ ). Furthermore, it is known from glass technology that in the case of spontaneous crystallization, taking place as soon as the melt is poured onto a steel plate, the length of time available to a melt for the formation and growth of crystals before it solidifies, is extremely short. Therefore, it can be assumed that the crystalline phases detected in the samples are those most probable to form, i.e. consisting of the elements most abundant in the melt or whose building blocks are already in location. Taking the above into account, unsurprising is the fact that spontaneous crystallization of materials from the CaO series starts with the formation of a compound out of constituents most abundant in the melt (i.e.  $\text{SiO}_2$ , CaO). It is noteworthy that until 3 mol.% of  $\text{SO}_3$  is added to the batch, the amount of detected  $\alpha$ -dicalcium silicate decreases. This observation indicates that sulphate addition influences the crystallization process of the studied materials, possibly by affecting the distribution (or availability) of the constituents

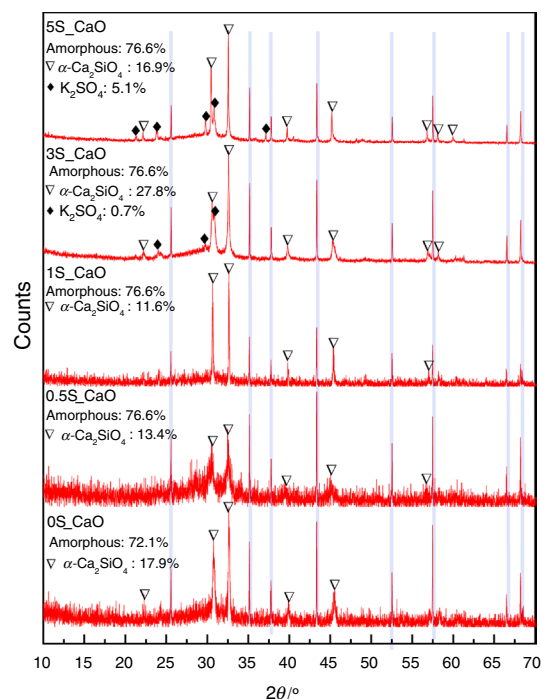


**Fig. 9** X-ray patterns of the samples representing CaO-series with the assignment of crystalline phases (the amount of corundum used as an internal standard was constant and equal 10 mass%)

needed to form a given compound. Once the nominal content of batched  $\text{SO}_3$  is equal 3 mol.%, besides the calcium silicate,  $\text{K}_2\text{SO}_4$  emerges in its crystalline form (Fig. 9). Judging by the rapid increase in the detected amount of calcium silicate, the precipitated sulphate may act as a nucleating agent, facilitating an overcoming the barrier of new nuclei formation and increasing the tendency of this very system to crystallize.

Similarly to the above-considered CaO series, the third system containing equal molar amounts of MgO and CaO was also found prone to spontaneous crystallization process (Fig. 10). However, interestingly enough, the particular diversity of crystalline phases, formed during this process, was discovered in the case of the dual system, which is believed to be a reflection of its highest compositional complexity among all studied series. From the XRD results, it follows that among the products of crystallization:  $\alpha$ -dicalcium silicate,  $\alpha$ -calcium potassium phosphate, as well as arcanite ( $\text{K}_2\text{SO}_4$ ) were detected. Despite the apparent intricacy of the succession of crystalline phases emergence as increasing sulphate content was loaded into the glasses, the same explanation as in the case of CaO system may be offered here. Once again then, the crystalline phases detected in the analysed samples are those, most probable to be formed, that is, the chemical composition and structure of which is close to this of material's microregions (domains

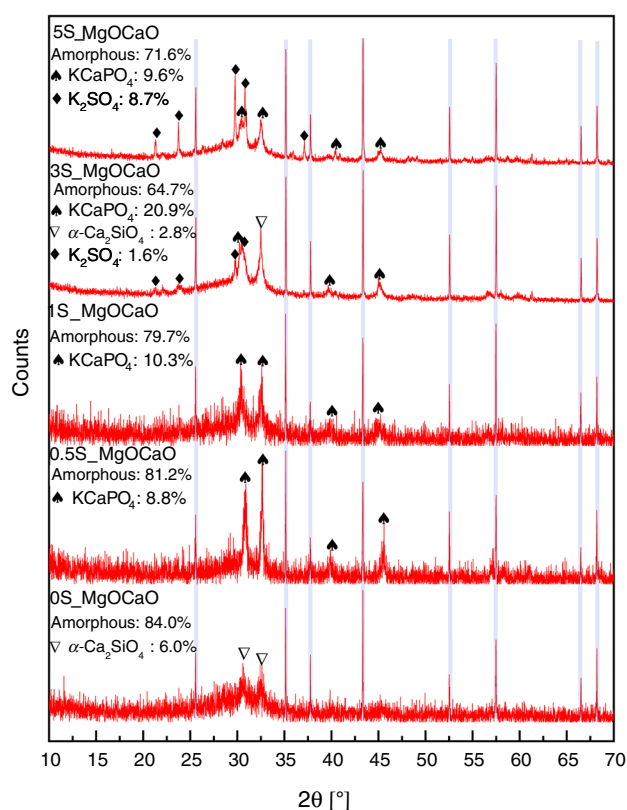


**Fig. 10** X-ray patterns of the samples representing the MgOCaO-series, with the assignment of crystalline phases (the amount of corundum used as an internal standard was constant and equal 10 mass%)

or clusters). Taking the above into account, the sequence of appearing of crystalline species with the increase in sulphate loading is unsurprising: at first (0–0.5 mol.% of  $\text{SO}_3$ ) those crystallites emerge, which are composed of the most abundant elements in the melt (Si, Ca, Mg, K), then (at 1 mol.% of  $\text{SO}_3$  loading) the effect of sulphate on the composition of glass microregions becomes apparent as only calcium potassium phosphate crystallizes, and finally, sulphur itself participates in the formation of crystalline phase ( $\text{K}_2\text{SO}_4$ ), as soon as the amount of batched  $\text{SO}_3$  reaches 3 mol.% (Fig. 10). Again it is believed that  $\text{SO}_3$  may act as a nucleating agent, as its presence drastically increases the amount of crystalline phases detected by the XRD technique.

As the next step in the characterization of as-synthesized materials in terms of their potential as glassy fertilizers, the thermal analysis was selected. It is because the results of such an analysis paradoxically may serve as a preliminary indicator of the biochemical activity of silicate-phosphate glasses. As stated by Waclawska et al. [8], an increase in the ability of such glasses for crystallization is a consequence of the weakened framework—a factor also responsible for the increase in their solubility in biological solutions. Thus, the

results of a comprehensive thermal investigation are demonstrated in the subsequent section.

### Thermal characteristics of synthesized materials (DSC study)

Characteristic glass temperatures, namely the glass transition temperature ( $T_g$ ), the crystallization onset ( $T_x$ ) and maximum temperature ( $T_c$ ), as well as the melting temperature ( $T_m$ ), determinable on the basis of the DSC technique, are widely acknowledged as being sensitive to any alteration in the chemical composition of the glass [26]. Indeed, as regards the MgO system, the effect of progressive sulphate addition into the structure of respective samples manifests itself on the DSC curves through systematic changes in the positions of glass transition effect, endothermic ( $T_m$ ) and exothermic peaks ( $T_c$ ) (Fig. 11, Table 3).

While the DSC curves of all glass samples from the MgO system show a distinct endothermic event associated with the glass transition, on those obtained for the MgOCaO one, this glass-specific phenomenon was only minor and hardly detectable (Fig. 12, Table 3). Analogously, the exothermic peaks originating from crystallization processes upon heating the samples were much less prominent than as regards glasses having only MgO as an alkaline earth modifier. A reasoning behind such an observation might be the partial crystallinity of the samples representing the dual system, and consequently—only a residual effect of vitreous state transformation.

Contrary to the above-considered glass compositions, on the DSC scans obtained for the CaO system no thermal effects have been recorded (Fig. 13). Such an observation should be treated as a clear indication of a significant amount of crystalline phase present in samples containing CaO as a glass modifier.

From the acquired DSC results of the systems exhibiting thermal effects (i.e. XS\_MgO, XS\_MgOCaO), several trends might be deduced. First and foremost, in all studied cases, the glass transition temperature increases together with an increase in the sulphate content, while the range of vitreous state transformation ( $T_{g\text{-endset}} - T_{g\text{-onset}}$ ) systematically decreases (Table 3). Nevertheless, although the above-mentioned tendencies are evident, the values of both those registered parameters in the analysed systems do not change radically. As regards the MgO-containing glass composition, a notable increment of  $T_g$  value, as well as reduction of  $T_g$  range, is not observed until after the  $\text{SO}_3$  content reaches 3 mol.%, while in the MgOCaO system the most significant increase in glass transformation temperature takes place as soon as the first portion of sulphate is introduced (0.5S\_MgOCaO sample).

It is known from the previous studies on the structure of sulphate-bearing glasses from the MgO system [27] that

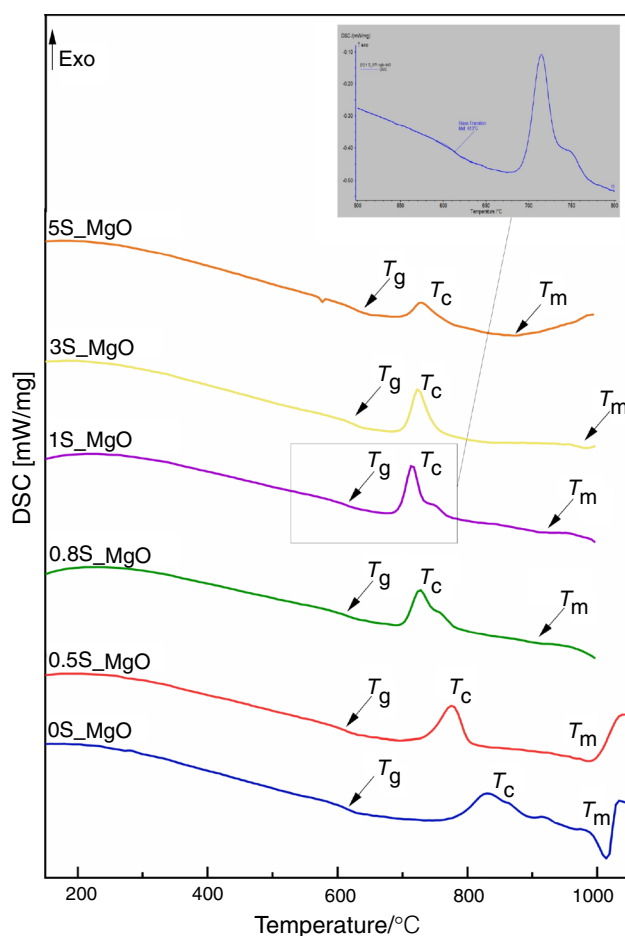


**Fig. 11** DSC curves of the sulphate-free and sulphate-bearing glasses from the MgO-system recorded at a heating rate of 10 °C/min. Upper-right corner: an exemplary determination of the glass transition temperature in the Proteus Software

**Table 3** Thermal characteristic of studied sulphate-bearing silicate-phosphate glasses

No	Characteristic glass temperatures/°C*						$\Delta H/J/g$
	$T_g$	$T_g$ range	$T_x$	$T_c$	$T_m$	$T_c$ range	
0S_MgO	614	35	785	831	1014	102	63.2
0.5S_MgO	612	35	737	776	987	63	64.9
0.8S_MgO	613	32	704	727	905	53	69.2
1S_MgO	613	37	696	715	919	38	67.2
3S_MgO	622	28	704	724	985	47	58.7
5S_MgO	636	19	704	728	875	63	32.8
0S_MgOCaO	627	21	697	717	986	46	29.9
0.5S_MgOCaO	646	22	719	739	999	62	28.3
1S_MgOCaO	649	15	737	760	1002	48	34.0
3S_MgOCaO	649	11	675	791	995	160	36.6
5S_MgOCaO	—	—	658	722	956	242	—**
				808	979		19.5

$T_g$  Glass transition temperature,  $T_x$  Temperature indicating an onset of glass crystallization,  $T_c$  Temperature at maximum crystallization peak,  $T_m$  Melting temperature,  $\Delta H$  Crystallization enthalpy

\*\*Evaluation of the  $\Delta H$  value has been unattainable in this case due to the limits related to small peak area

$SO_3$  introduction impairs a slightly polymerizing effect on the silicate subnetwork. Therefore, an observed increase in the  $T_g$  values in this glass composition appears to be justified. Although an analogous explanation may be offered to the dual  $MgOCaO$  system, it needs to be recalled that materials representing this very composition display partial crystallinity (see “X-ray diffraction analysis” section). The consequence of the glassy-crystalline state is the higher degree of ordering due to the precipitation of crystallites and subsequently the reduced flexibility of the molecular chains of the material. Therefore, the noticed increment of the temperature, at which the material changes from a glassy state to a highly elastic state, may also be an effect of increased rigidity of the structure, caused by the presence of crystalline domains.

The aforementioned narrowing of vitreous state transformation range (i.e. decrease in relaxation time), in both analysed systems, corroborates the theory of increasing rigidity of materials’ internal structure together with an increase in  $SO_3$  content. It is known from the study of Stoch [28, 29] that shortening of the time needed for a relaxation of structural strains may indicate that this process takes place through breaking of chemical bonds (a process peculiar to rigid bodies) rather than a displacement of structural units without disturbing the continuity of the network (characteristic for flexible structures).

As regards the exothermic peaks identified on the DSC curves of glasses from the MgO system (Fig. 11, Table 3), it may be seen that the registered onset of crystallization process ( $T_x$ ) shifts towards lower temperatures with an increase in the  $SO_3$  addition level (from 785 °C for sulphate-free sample, by nearly 740 °C at 0.5 mol.%, to ~700 °C at higher  $SO_3$

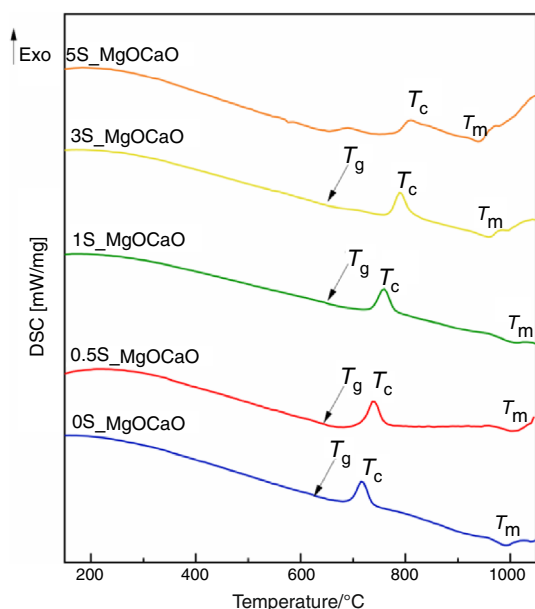


**Fig. 12** The DSC traces of the glasses representing the MgOCaO system, recorded at a heating rate of 10 °C/min

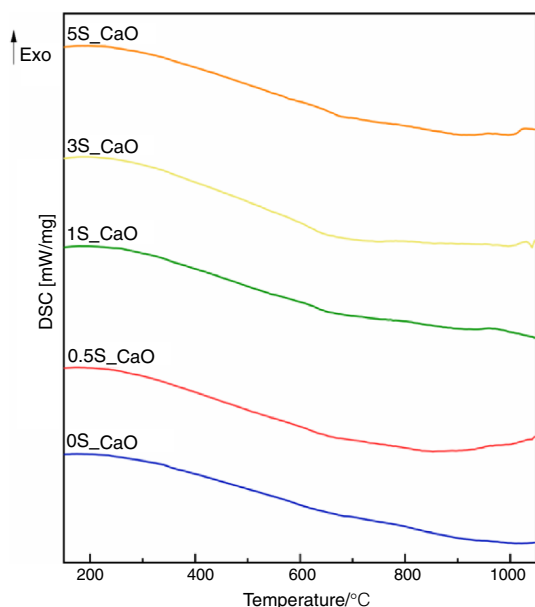


**Fig. 13** DSC curves of the sulphate-free and sulphate-bearing glasses from the CaO-system recorded at a heating rate of 10 °C/min

addition levels). Noteworthy is the fact that besides the  $T_x$ , also the heat of crystallization is altered by sulphate loading. Its initial gradual growth is followed first by a slight decrease, after 1 mol.% of sulphate has been introduced to the glass composition and then by a rapid reduction, as regards the sample with 5 mol.% of SO<sub>3</sub> added (Table 3).

This almost halved, compared to the starting value, enthalpy of crystallization, measured for the 5S\_MgO sample, is reasonable when the semicrystallinity of this material is taken into consideration. Then, during the heating in the course of the DSC measurement already smaller fraction of the amorphous phase is susceptible to crystallization. Also worth mentioning is the changing shape of DSC exothermic peak, together with an increase in SO<sub>3</sub> content. It is evident (Fig. 11) that compared to the sulphate-free sample, it becomes more narrow and sharp already at 0.5 mol.% of sulphate. This phenomenon, according to Stoch et al. [30], is indicative of the change of crystallization kinetics as a result of sulphate loading, starting from slow to faster. Meanwhile, in the XS\_MgOCaO system the onset of crystalline phases formation goes up at first, only to decline once the SO<sub>3</sub> content reaches 3 mol.% (Table 3). It should also be emphasized that at this threshold value of sulphate content the crystallization phenomenon changes its course and becomes a two-stage process. And while the observed initial increase in the  $T_x$  along with SO<sub>3</sub> content in all likelihood is attributed to the semicrystallinity of the respective samples, for the aforementioned change of crystallization mechanism the SO<sub>3</sub> addition may be held responsible. Analogously to the MgO series, although the heat of crystallization ( $\Delta H$ ) does not change rapidly along with sulphate addition (Table 3), a notably upward trend persists, until 3 mol.% is SO<sub>3</sub> is introduced to the batches. The rapid decrease in  $\Delta H$  once this loading content has been reached is correlated with the change of the crystallization course to two-stage process.

From the foregoing considerations, it follows that the introduction of SO<sub>3</sub> into both of the analysed systems increases the propensity of materials to undergo crystallization, which is manifested by lowering the onset of this process as well as the change of its mechanism. To reveal more information concerning this apparent tendency towards devitrification, the process of induced crystallization was performed, based on the temperatures at maximum of DSC exothermic effects. The results of such experiment are presented in “X-ray diffraction study of devitrificates” section.

Meanwhile, attention should be given to the fact that in the temperature range preceding the glass transformation region an additional endothermic peak emerges on the DSC curves of 5S samples (i.e. 5S\_Mg sample, Fig. 11; 5S\_MgO-CaO sample, Fig. 12). The specificity of this particular feature suggests the phase transformation of a certain glass component. As revealing the nature of this effect would shed more light on the changes taking place in the structure of studied materials as a result of sulphate addition, its origin will be discussed in detail in the next part of the present paper.



## HT-XRD study

As a method enabling an investigation of the nature of the distinctive endothermic peak emerging on the DSC curves of 5 mol.% sulphate containing glasses (5S\_MgO, 5S\_MgOCaO, Figs. 11, 12) at about 577 °C, the HT-XRD analysis has been selected. Consequently, in Figs. 14, 15, the sequence of X-ray diffractograms recorded for the temperature interval of 25–600 °C, during the heating and cooling cycles of the analysed sample have been presented.

At first, it should be emphasized that on all the acquired diffraction patterns  $\text{Al}_2\text{O}_3$  originating from the corundum sample holder of the XRD apparatus demonstrates its presence by sharp reflections marked with an asterisk (Figs. 14, 15). Apart from this fact, the HT-XRD results corroborate those collected by the room-temperature XRD (see “X-ray diffraction analysis” section) denoting that the only crystalline phase present in the 5S\_MgO sample at ambient temperature (25 °C) is potassium sulphate (VI). Nevertheless, a gradual increase in the measurement temperature provokes certain changes in the structure of the studied material, which clearly manifest themselves on the respective XRD patterns. Particularly notable is small displacement of  $\text{K}_2\text{SO}_4$  peak positions toward lower  $2\theta$  angle, which can be explained by the expansion of the crystal structure [31], but of the utter importance is the emergence of supplementary XRD reflections at the expense of the initial ones. Preliminary evidence of the latter constitutes diffractogram recorded at 575 °C on which diffracton peaks, additional to the already existing, appear

at  $2\theta$  values of 22.0 and 44.9°. As a consequence of the further heat treatment, not only an increase in relative intensities of the aforementioned reflections is observed, but also a minor peak localized at 28.2°  $2\theta$  becomes sharp and prominent, while reflections originally positioned at 26.3, 29.8, 35.9, 37.1, 40.4, 40.9 and 48.7° fall gradually in intensity with temperature and disappear altogether above 590 °C. Importantly, upon cooling the sample to initial temperature of 25 °C (patterns shown in Fig. 15), the just developed peaks revert fully to their original positions.

The above-presented results provide a simple explanation of the observed changes in XRD patterns and concomitantly the occurrence of endothermic peak on the DSC curves, which is as follows: the  $\text{K}_2\text{SO}_4$  phase detected at ambient temperature is present in its orthorhombic form (Pnma unit cell), stable up to temperature of approximately 575 °C, at which its hexagonal polymorph (P63/mmc unit cell) appears in the assemblage and becomes an only phase above 590 °C. Cooling the system to room temperature reverts the  $\beta\text{-K}_2\text{SO}_4 \rightarrow \alpha\text{-K}_2\text{SO}_4$  transformation, corroborating at the same time the DSC results (Figs. 11, 12, Table 4).

As a final point of the analysis of HT-XRD results, attention should be paid to the appearance of minor reflection on the diffractograms (27.4°) recorded at temperatures above 400 °C (Fig. 14). Detailed investigation of the origin of this particular feature indicated that it is related neither to  $\text{K}_2\text{SO}_4$  nor to  $\text{Al}_2\text{O}_3$ , but rather to potassium magnesium phosphate (Table 4). The presence of the detected phase is, in all probability, a consequence of the specificity of the experiment itself, as the studied sample was maintained for a period of

**Fig. 14** In situ HT-XRD patterns of 5S\_MgO sample at various temperatures, during heating cycle. The diffraction peaks denoted by closed and open circles and closed diamonds could be identified as  $\beta\text{-K}_2\text{SO}_4$ ,  $\alpha\text{-K}_2\text{SO}_4$  and  $\text{KMgPO}_4$ , respectively. The peaks represented by an asterisk are originating from the  $\text{Al}_2\text{O}_3$  sample holder of the XRD apparatus

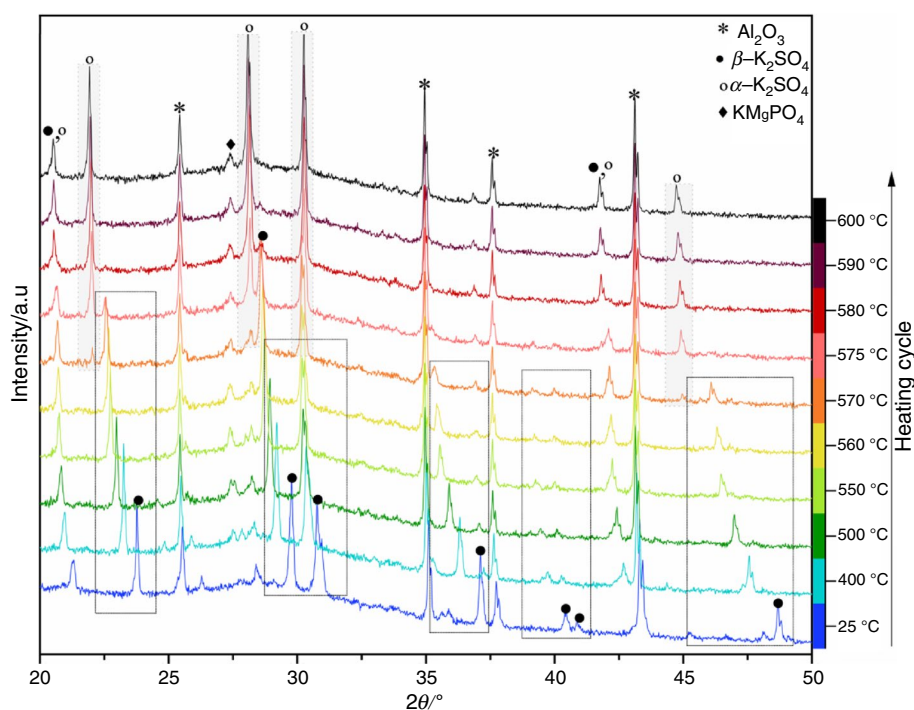
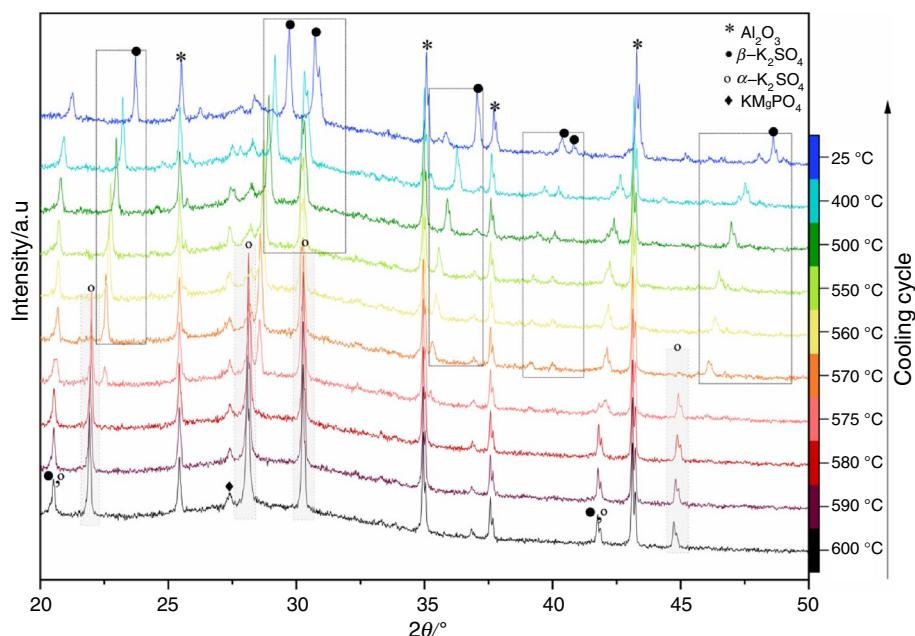


**Fig. 15** In situ HT-XRD patterns of 5S\_MgO sample at various temperatures, during cooling cycle. The diffraction peaks denoted by closed and open circles and closed diamonds could be identified as  $\beta$ -K<sub>2</sub>SO<sub>4</sub>,  $\alpha$ -K<sub>2</sub>SO<sub>4</sub> and KMgPO<sub>4</sub>, respectively. The peaks represented by an asterisk are originating from the Al<sub>2</sub>O<sub>3</sub> sample holder of the XRD apparatus



time at a particular temperature during the heating/cooling cycle. It may then be assumed that such measurement conditions favoured formation of the crystalline phase, here, in the form of KMgPO<sub>4</sub>.

#### Estimation of thermal stability of synthesized materials

Besides the long-known thermal characteristics of glassy materials based on the set of three specific temperatures, namely glass transition, glass crystallization and glass melting, there is also a complementary approach, in which the relative positions of those effects are used to evaluate the thermal behaviour of glasses. In fact, many researchers, in order to enable a direct comparison between various types of glasses, developed certain formulas, numerically expressing the thermal stability of glasses [22]. And although such parameters, nowadays referred to as glass stability (GS) parameters, by definition carry information about the stability of glass against devitrification on heating, some researchers [1, 22, 32] argue that few of them may also be used to conclude about glass-forming ability (GFA) of studied materials—the parameter which is usually assessed based on critical cooling rate of the melt. Therefore, to complement the thermal characteristics of obtained glassy and glassy-crystalline samples given in the Sect. 3.1.4, the Turnbull ( $K_T$ ) [23], Angell ( $K_A$ ) [1], Hruby ( $K_H$ ) [22], Weinberg ( $K_W$ ) [1] as well as Lu and Liu ( $K_{LL}$ ) [24] parameters have been calculated, and the results are presented in Table 5. It should be recalled here that because the DSC curves of the CaO-containing system do not display any thermal effects specific for the glassy state, materials representing this very system are not taken into account in the following considerations.

**Table 4** Summary of the HT-XRD analysis

Temperature/°		Phase	Reference code
25	Heating	Corundum	98-002-4851
		Dipotassium sulphate (VI), Arcanite	00-024-0703
600		Corundum (HT)	98-016-0606
		Potassium sulphate (VI) (HT)	01-070-1227
		Potassium Magnesium Phosphate (HT)	00-050-0151
25	Cooling	Corundum	98-002-4851
		Potassium sulphate (VI)	00-024-0703
		Potassium Magnesium Phosphate	00-050-0146

One of the earliest proposed and widespread parameters, characterizing the capability of materials to exist in glass form is the reduced glass transition temperature, firstly suggested by Kauzmann and later studied by Turnbull (hence known also as Turnbull parameter,  $K_T = T_g/T_m$ ) [23]. It is founded on the simple assumption that a liquid with a high viscosity between  $T_g$  and  $T_m$  typically displays significant glass-forming properties with no need to provide a high cooling rate of the melt. And since the viscosity of oxide glasses is nearly constant at  $T_g$  ( $\sim 10^{13}$  Pa s) [22], it was suggested that the higher the value of the reduced glass-transition temperature, the higher the viscosity in the undercooled liquid state, and subsequently, the lower cooling rate would be required to bypass crystallization of the melt during cooling. Additionally, postulated was the fact that if  $K_T$  value is greater than or equal to 2/3 ( $\sim 0.67$ ), the process of homogenous nucleation will be kinetically suppressed. Therefore, judging by the calculated values of the  $K_T$  for the

studied materials, which, as can be seen in Table 5, oscillate around the threshold value of  $\sim 0.67$ , it may be inferred that although for all those glass compositions the condition under which a glassy material can be formed is fulfilled, the higher cooling rates would be advantageous to ensure that the crystallization process is bypassed. Also worth attention is the fact that the as-defined glass forming ability firstly increases for the MgO system, only to decrease as soon as the sulphate content reaches 3 mol.%. This observation may be treated as an indication of a threshold sulphate loading before crystallization takes place in this very system. A final conclusion which may be drawn from the Turnbull parameter concerns the preferred crystallization mechanism by which the crystallization of analysed glasses takes place. Following Zanolto's considerations [33], according to which glasses exhibiting  $K_T$  value lower than 0.58–0.60 show only volume (homogeneous) nucleation, while those displaying surface (mostly heterogeneous) crystallization are characterized by  $K_T > 0.58$ –0.60. If it is a case, together with the increase in sulphate content in all analysed systems, surface crystallization becomes a predominant factor contributing to the devitrification process.

As regards the theoretical estimation of the glass stability (GS) upon heating, Angell was probably the first to suggest a numerical measure for this very parameter, which was a simple difference between crystallization and transformation temperatures ( $K_A = T_x - T_g$ ) [1, 34]. The term ( $T_x - T_g$ ) in the proposed formula expresses the resistance of a obtained material to crystallization, and the smaller this interval, the higher its tendency to crystallize. In light of the foregoing, the calculated values of the Angell parameter (Table 5) unambiguously imply that in both the MgO- and the MgO and CaO-containing systems the propensity of materials towards crystallization increases together with sulphate loading.

The remaining three GS parameters (Table 5), namely the Hruby ( $K_H = (T_x - T_g)/(T_m - T_x)$ ) [22], the Weinberg ( $K_W = (T_x - T_g)/T_m$ ) [1] and the Lu and Liu ( $K_{LL} = T_x/(T_g + T_m)$ ) [24], are similar in the sense that each of them is expressed by certain configuration of three DSC characteristic temperatures ( $T_g$ ,  $T_x$  or  $T_c$  and  $T_m$ ). It has been established that the higher the values of the aforementioned parameters, the higher is the stability of a glass against devitrification on heating [35]. Furthermore, worth emphasizing is the fact that, as indicated by an extensive study carried out by Nascimento et al. [1], all the three above-mentioned formulas allow one to deduce not only the glass stability of the analysed material, but also its glass-forming ability, defined as the easiness to vitrify a liquid on cooling given that the results presented in Table 5 clearly suggest that a progressive increase in sulphate content in the structure of MgO-containing glasses results in a subsequent decrease in GS as well as GFA. An exception to this rule constitutes the 5S\_Mg sample, showing noticeably higher values of  $K_H$ ,  $K_W$  and  $K_{LL}$  parameters. The possible explanation to this phenomenon may lie behind the partial crystallinity of this very material and consequently the higher stability of the remaining amorphous phase. The same explanation might be offered to the MgOCaO system, exhibiting the opposite relationship between the  $\text{SO}_3$  content and the values of the calculated parameters (Table 5), than the MgO-containing one. As the amount of crystalline phase in the materials representing this system increases together with sulphate loading, the estimated glass stability increases in the same manner, manifesting at the same time a superior stability of a glass-crystalline materials compared to the fully amorphous ones.

Although the above-presented considerations concerning glass thermal parameters should be treated with caution as they depend on the value of  $T_g$ , known to be sensitive to

**Table 5** Values of the glass stability parameters calculated for the analysed materials

No	The kind of parameter				
	Turnbull/ $K_T$	Angell/ $K_A$	Hruby/ $K_H$	Weinberg/ $K_W$	Lu and Liu/ $K_{LL}$
0S_Mg	0.605	171.6	0.749	0.214	0.482
0.5S_Mg	0.621	124.8	0.500	0.166	0.461
0.8S_Mg	0.677	91.1	0.453	0.126	0.464
1S_Mg	0.667	82.7	0.371	0.111	0.454
3S_Mg	0.632	81.5	0.290	0.103	0.438
5S_Mg	0.727	68.3	0.400	0.105	0.466
0S_MgCa	0.635	70.7	0.245	0.092	0.432
0.5S_MgCa	0.647	72.6	0.259	0.093	0.437
1S_MgCa	0.647	88.4	0.333	0.111	0.446
3S_MgCaO*	0.679	25.8	0.092	0.076	0.420

\*In the calculations of the glass stability parameters for the 3S\_MgOCaO sample displaying two-stage crystallization, the temperature of the first exothermic effect was taken into consideration, as it indicates the onset of the whole process

preparative conditions of glass formation or the thermal history of glass [35], the obtained results certainly give a close approximation of the glass-forming tendency of the studied materials [1, 32, 35]. It may clearly be deduced that in the MgO system, together with sulphate content, glass-forming properties as well as resistance to devitrification of materials diminish progressively. Moreover, such a trend persists until more than 3 mol.% of  $\text{SO}_3$  is added to the glass composition (Fig. 16). After this threshold value is exceeded, increased values of the glass stability parameters are manifestation of the presence of a crystalline phase. Such results allow to infer that it is the  $\text{SO}_3$  addition into the structure of MgO-containing glasses that affects their crystallization tendency. On the other hand, parameters acquired for the glassy crystalline materials representing the MgOCaO system show opposite trend than those representing the MgO-containing one, but likewise, this tendency changes its course after a certain value (1 mol.% of  $\text{SO}_3$  content) is reached (Fig. 16). An while this initially rising trend is a consequence of the partially crystalline form of the materials acquired in this very system and consequently an improved thermal stability over their fully amorphous counterparts, a reasoning behind the sudden change of its direction may be found in the alteration of the course of crystallization to two-stage process with which it correlates.

Besides considerations on sulphate content effect on the glass forming tendencies of studied systems, there is also

one more factor that should be taken into account. The factor referred to is the type of alkaline earth modifier present in a given series. Both MgO and CaO, despite apparent similarity as the ionic radii of  $\text{Mg}^{2+}$  (0.72 Å) are close to ionic radii of  $\text{Ca}^{2+}$  (0.99 Å) [36], behave differently when enter the glass structure. And while the CaO acts exclusively as a network modifier, weakening the glassy framework by its depolymerization, the role of MgO is concentration dependent [37]. It is believed that magnesium oxide, when present at high concentration, may act as a network intermediate and enter the silicate network, decreasing the number of NBOs (non-bridging oxygens) as well as increasing NC (network connectivity) at the same time. These above-presented differences in properties of both oxides should not be neglected in considerations on glass forming ranges of studied systems. It needs to be recalled that batches characterized by the presence of CaO, either as sole (CaO series) or supplementary (MgOCaO series) alkaline earth oxide, displayed noticeably low viscosity (explicable in light of depolymerizing effect of this oxide) when pouring the melt and consequently the utmost propensity for spontaneous crystallization.

On the other hand, there is the MgO system containing magnesium oxide as a sole alkaline earth component and exhibiting the broadest glass forming range of all the studied series. Such result is not exceptional when one takes into account the literature data presenting analogous results. As reported by Waclawska et al. [38], while in the

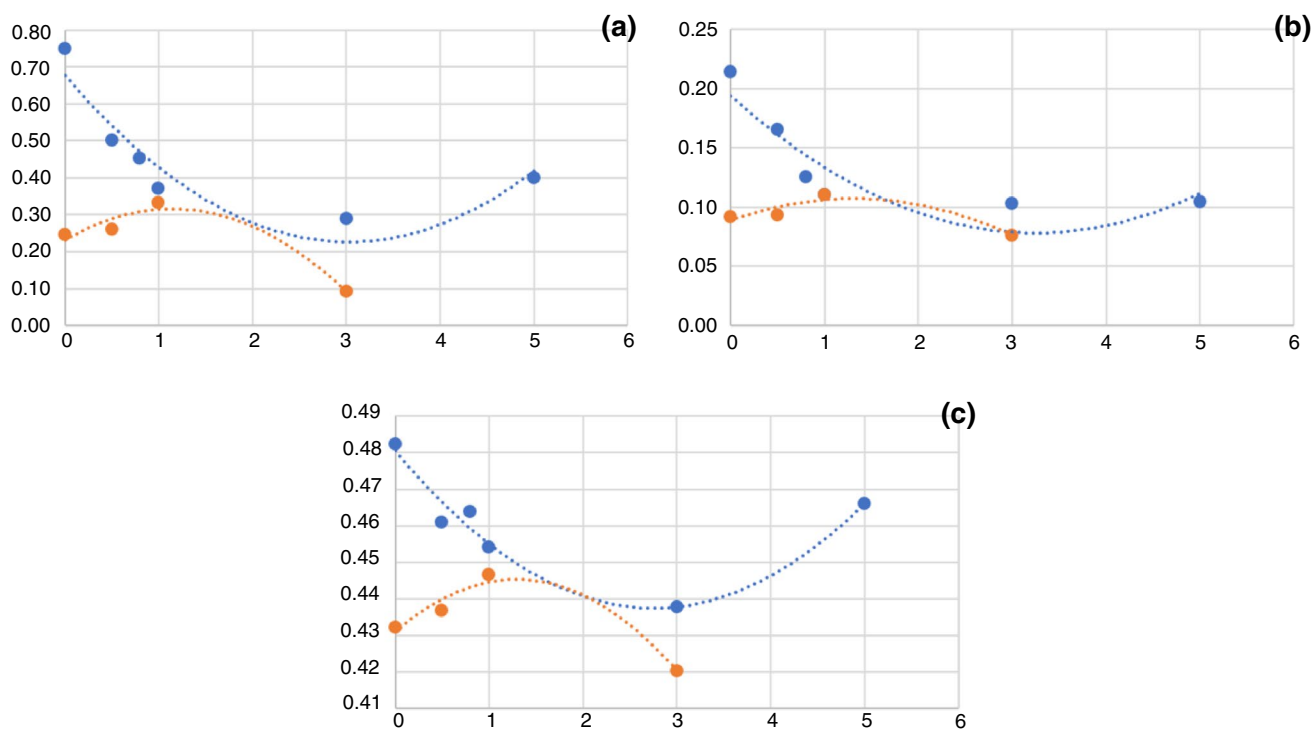


**Fig. 16** The calculated values of selected thermal parameters (Hrubý (a), Weinberg (b), Lu and Liu (c)) obtained for the analysed systems: MgO-system (blue line) and MgOCaO-system (orange line). Only the parameters having considerable correlation with the GFA has been plotted



silicate–phosphate glasses containing a modifier in the form of  $\text{Mg}^{2+}$  ions, their ability to crystallize does not appear until the value  $\text{MgO}/\text{SiO}_2 = 0.61$ , in those containing  $\text{Ca}^{2+}$  ions as a modifier, crystallization is observed already at the value  $\text{CaO}/\text{SiO}_2 = 0.24$ . It is also valuable to share the results of Watts et al. [39], who presumed that the presence of magnesium in silicate–phosphate-based glasses increases their resistance to crystallization. It may be then stated that it is the presence of MgO that aids in acquiring fully amorphous samples in the studied sulphate-bearing silicate–phosphate glasses, while the presence of CaO, by lowering melt viscosity, conduces their spontaneous crystallization.

## Devitrified materials

### X-ray diffraction study of devitrificates

It is known from the thorough studies on multicomponent silicate–phosphate glasses that the process of glass devitrification progresses by the reorientation of domains upon the heat treatment. Furthermore, such domains may be viewed as crystallization nuclei, determining the type of crystallizing phases [12, 40, 41]. Owing to this apparent dependency between the character of groupings present in the glass and the type of crystalline compounds emerging under heat treatment, an outcome of the induced crystallization process may shed some light on the domain structure of studied materials. It must be emphasized here that the kind of domains existing in the structure of glassy fertilizers is of utter importance, as it constitutes a significant factor determining their chemical activity in biological solutions [42]. Therefore, an induced crystallization process was performed on the as-synthesized samples and the resulting phase composition of such devitrificates is demonstrated below (Table 6).

At first, it should be mentioned that the detected crystalline phases differ significantly from those identified in the case of as-synthesized samples. It is logical given an incomparably longer time available for the isothermally heated glasses for crystal growth, in relation to the time available for those materials during solidification of a melt. Moreover, when comparing both the acquired XRD results, it is useful to remember that during heat treatment of the obtained glass, the nuclei form in the glass transformation range and grow in the temperature range of the exo-peak, while as it cools, the melt with a small number of nuclei first crosses the region of high growth rate [32] given that it is justifiable that the spontaneous crystallization proceeds differently than the induced one, along with an increase in  $\text{SO}_3$  content.

It may be stated that several factors govern the course of the crystallization process of sulphate-bearing glasses. The first one is actually sulphate addition itself, which, as has been demonstrated previously, clearly influences the tendency of studied glasses to crystallize. It is useful to recall

that incorporation of increasing amounts of  $\text{SO}_3$  not only lowers the onset temperature of the crystallization process, but also affects its mechanism and enhances the degree of crystallinity of studied materials. Another consequence related to sulphate of its incorporation is the emergence of  $\text{K}_2\text{SO}_4$ , as soon as a considerable amount of sulphate is added to the batches. This particular phase is detected at 5 mol.% of introduced  $\text{SO}_3$  in the MgO-containing glass composition, and already at 1 mol.%, as regards the dual system (Table 6). It is also of utter importance to notice that sulphur does not participate in any of the detected crystalline phases, besides the above-mentioned potassium sulphate. This observation corroborates the results demonstrated in the previous study on the structure of sulphur-bearing glasses [27], in which it was stated that sulphur in multicomponent glasses exists as independent units, not linked to the silicate–phosphate network. Another factor affecting the crystallization process of multicomponent glasses is crystallochemical one, which, as follows from thorough research [2, 43, 44], highly influences the type of emerging crystalline compounds. According to those studies, this crystallochemical factor corresponds to the strength of chemical bonds between given cations and oxygen linking them and may be expressed numerically by the difference in the value of the ionicity of bonds ( $i_G$ ) between oxygen and the relevant cations. It also should be mentioned that the smaller the difference in the bonds' ionicity ( $\Delta i_G$ ), the lower will be the strength of the oxygen bridges, and therefore the easier those bonds will be broken in the course of the crystallization process. The effect of crystallochemical factors is especially well pronounced as regards the MgO series (Table 6). As the linkages of the K–O–Si ( $\Delta i_G$ : 0.395) or Mg–O–Si ( $\Delta i_G$ : 0.241) type are weaker than the bonds within the silicate subnetwork itself, and additionally, weaker than the analogous linkages with phosphorus: K–O–P ( $\Delta i_G$ : 0.511) or Mg–O–P ( $\Delta i_G$ : 0.357), they are easily disrupted during heat treatment. Consequently, the components released from the silicate subnetwork are now able to form separate crystal phases. This, in turn, is reflected in the kind of crystallizing compounds—in the case of all sulphate-bearing samples undergoing crystallization in lower temperatures range, only phosphates were detected by the XRD analysis ( $\text{KmgPO}_4$  and  $\text{Mg}_2\text{P}_2\text{O}_7$  only in the 3S\_MgO sample), naturally with the exception of the 5S\_MgO sample, containing also the  $\text{K}_2\text{SO}_4$  phase, while in the sulphate-free sample crystallizing at highest temperature, when the diffusion processes are intensive enough, besides phosphate phase ( $\text{KmgPO}_4$ ), also two different silicates emerge ( $\text{Mg}_2\text{SiO}_4$ ;  $\text{K}_{1.14}\text{Mg}_{0.57}(\text{Si}_{1.43}\text{O}_4)$ ). When discussing crystallochemical factors, it is also interesting to state after Stoch [29] that the difference in ionicity of bonds  $\Delta i_G$  in the oxygen bridge may also be a measure of acid–base interactions in this bridge and hence gives a certain evaluation of

**Table 6** Types of crystalline products detected in the XRD-analysed materials

No	Crystalline phase	Reference code	Mineral name
0S_MgO	$K_{1.14}Mg_{0.57}(Si_{1.43}O_4)$	00-044-0089	Potassium Magnesium Silicate
	$Mg_2SiO_4$	00-004-0769	Forsterite
	$KMgPO_4$	98-005-0926	Potassium Magnesium Phosphate (V)—Alpha
0.5S_MgO	$KMgPO_4$	00-050-0149	Potassium Magnesium Phosphate
0.8S_MgO	$KMgPO_4$	00-050-0149	Potassium Magnesium Phosphate
1S_MgO	$KMgPO_4$	00-050-0149	Potassium Magnesium Phosphate
3S_MgO	$KMgPO_4$	00-050-0149	Potassium Magnesium Phosphate
	$Mg_2P_2O_7$	00-005-0579	Magnesium Phosphate Oxide
5S_MgO	$KMgPO_4$	00-050-0149	Potassium Magnesium Phosphate
	$K_2SO_4$	00-003-0608	Dipotassium sulphate
0S_MgOCaO	$KCaPO_4$	00-033-1002	Potassium Calcium Phosphate
	$K_2MgSi_3O_8$	00-019-0973	Potassium Magnesium Silicate
0.5S_MgOCaO	$KCaPO_4$	00-033-1002	Potassium Calcium Phosphate
	$K_2MgSi_3O_8$	00-019-0973	Potassium Magnesium Silicate
1S_MgOCaO	$KCaPO_4$	00-033-1002	Potassium Calcium Phosphate
	$K_2MgSi_3O_8$	00-019-0973	Potassium Magnesium Silicate
	$K_2SO_4$	00-003-0608	Dipotassium sulphate
3S_MgOCaO	$K_{1.14}Mg_{0.57}(Si_{1.43}O_4)$	00-044-0089	Potassium Magnesium Silicate
	$KCaPO_4$	00-033-1002	Potassium Calcium Phosphate
	$K_2MgSi_3O_8$	00-019-0973	Potassium Magnesium Silicate
	$CaMgSiO_4$	01-084-1320	Monticellite
	$K_2SO_4$	00-003-0608	Dipotassium sulphate
5S_MgOCaO	$KCaPO_4$	00-033-1002	Potassium Calcium Phosphate
	$K_2MgSi_3O_8$	00-019-0973	Potassium Magnesium Silicate
	$Ca_2KP_3O_{10}$	00-040-0190	Potassium Calcium Phosphate
	$Mg_2P_2O_7$	00-005-0579	Magnesium Phosphate Oxide
	$K_2SO_4$	00-003-0608	Dipotassium sulphate

local chemical affinity of joined cations to oxygen. Therefore, given that the  $\Delta i_G$  of S–O–K, S–O–Ca and S–O–Mg is 0.621, 0.505 and 0.467, respectively, it is unsurprising that it is  $K_2SO_4$  that crystallizes once the sulphate capacity of glass is exceeded.

And while the crystallochemical factor well explains the type of crystallizing phases in the simpler systems, such as MgO series, the sequence of crystalline products formation in the dual system, in which both alkaline earth modifiers have comparable values of  $i_G$  ( $i_G$  of MgO: 0.671;  $i_G$  of CaO: 0.708), finds better interpretation in the chemical affinity of components participating in the synthesis. A numerical expression of such an affinity may constitute the Gibbs free energy of formation of both silicates and phosphates from oxides ( $\Delta G$ ) [45]. It should be mentioned that among the numerous reactions that can proceed in a given system, a reaction characterized by the least value of  $\Delta G$  occurs with the highest probability.

Indeed, the  $\Delta G$  values calculated for the silicates that can crystallize in the analysed materials (Table 7) well explain the kind of phases appearing in the MgOCaO series, during

induced devitrification. In all samples representing this very system, it was precisely  $K_2MgSi_3O_8$  (i.e. a silicate compound of the lowest  $\Delta G$  value) that was identified in the respective XRD patterns, while other detected silicates ( $K_{1.14}Mg_{0.57}(Si_{1.43}O_4)$ ;  $CaMgSiO_4$ ) did not emerge, until the induced crystallization was performed in the higher temperatures range. Nevertheless, the comparison of the  $\Delta G$  values acquired for phosphates demonstrates that the chemical affinity reflected by the Gibbs free energies of formation, again, is not the sole factor determining the appearance of crystalline compounds and should be considered with knowledge of the structure of a given material. From the previous studies on the glasses of corresponding composition, it follows that the phosphate subnetwork consists of both the ortho- and diphosphate units, with the substantial prevalence of the former [27]. Given that it is unsurprising that among all the possible phosphates (Table 7), it is  $KCaPO_4$  that crystallizes in each sample from the MgOCaO system. Also worth attention are the sulphate compounds that can be expected to form from the elements present in the melt of studied compositions (Table 7). It is intriguing, that

although  $\text{CaSO}_4$  is characterized by the lowest value of  $\Delta G$ , precisely  $\text{K}_2\text{SO}_4$  appears in the assemblage as a sulphate-bearing phase. An explanation behind this unexpected observation may lie in the fact that judging by the calculated  $\Delta G$  values (Table 7 *Values of  $\Delta G$  of the formation of exemplary simple silicates and phosphates*), both  $\text{CaO}$  and  $\text{MgO}$  have stronger chemical affinity to  $\text{P}_2\text{O}_5$  and/or  $\text{SiO}_2$  than  $\text{K}_2\text{O}$ , and hence, they preferably participate in the formation of silicate and/or phosphate phases over the sulphate ones.

In connection with the previously mentioned parallelism between the domain structure of glass and a kind of crystallizing compounds upon its heat treatment it may be stated that in the materials representing both systems there exist groupings of the orthophosphate type, namely  $\text{KMgPO}_4$  as regards the  $\text{MgO}$  series and  $\text{KCaPO}_4$  in the case of the dual one. Furthermore, judging from the crystallization products of the samples from the analysed systems, the groupings based on silicate units accompany those, corresponding to the orthophosphate-like. It is of utter importance in terms of the potential application of the studied materials as glassy fertilizers, since the formation of domains with a silicate-type structure is indispensable for the increase in the biochemical activity of glasses [42]. Worth particular attention is the fact that sulphur does not participate in any of above-mentioned domains, but apparently forms independent groupings of the  $\text{K}_2\text{SO}_4$ -type, and in this particular form it precipitates at 5 mol.% of introduced  $\text{SO}_3$  in the

$\text{MgO}$ -containing glass composition, and already at 1 mol.%, as regards the dual system.

The particular significance of the type of ordering as regards glassy carriers of micro- and macroelements inclined the authors to deepen the above-presented investigation and exploit the potential of the Raman spectroscopy imaging (RSI) method. The acquired results are revealed in the following section.

## Raman Imaging analysis

Due to very high resolution and a possibility to generate chemical images from point by point-taken spectra, it was Raman spectroscopy imaging (RSI) that has been selected as a technique to study cluster distribution and origin in the obtained devitrificates. Such mapping procedure was performed on the samples from both the  $\text{MgO}$  and  $\text{MgOCaO}$  series, characterized by the highest sulphate content (i.e. 3S\_MgO, 5S\_MgO, 3S\_MgOCaO, 5S\_MgOCaO), and the resulting images together with the Raman spectra taken at different regions of analysed profiles are depicted in the Figs. 17–20. Additionally, in order to facilitate tracking the changes which emerged as a result of thermal treatment, each spectral assemblage is supplemented with a spectrum of initial, as-synthesized material. Moreover, with the purpose of rendering the below considerations more comprehensible, the assignment of vibrational modes characteristic for units present in studied multicomponent silicate-phosphate glasses has been demonstrated in Table 8, while more in-depth discussion of the structure of such materials is comprised in the previous study by the authors [27].

Preliminary investigation of the RSI results acquired for the  $\text{MgO}$  series indicates that studied devitrificates from this system resemble each other to a certain extent. It is because the dominant (matrix) phase, present on the analysed profiles of both samples, has the same nature, which is manifested by the similarity of respective Raman spectra taken at the regions denoted as Component 1 (Fig. 17 red spectrum, Fig. 18 red spectrum). The presence of sharp bands of narrow half-width, overlapped on the broader ones characteristic for amorphous phase, is indicative of partially crystalline nature of this very region of analysed samples—a consequence of their thermal treatment. Thorough examination of wavenumber positions of the spectral features allows to state with some confidence that the Component 1 constituting the majority of both materials, although predominantly consists of amorphous phase, contains also certain amount of  $\text{KMgPO}_4$  (identified by the high-intensity bands at about 970, 995 and 1030  $\text{cm}^{-1}$ ) and  $\text{K}_2\text{SO}_4$  (identified by the bands near 980, 618, 453  $\text{cm}^{-1}$ ) crystallites [47–49]. It is worth emphasizing that the identified phases correspond to those detected by the XRD examination. Besides the above-mentioned, on the studied profile of the 3S\_MgO sample one can

**Table 7** Calculated Gibbs free energies of the formation of compounds from the oxides [46]

Crystalline phase		$\Delta G_f^0/\text{kJ/mol}$	
		1000 K	1100 K
Silicates	$\text{K}_2\text{MgSi}_3\text{O}_8$	−4100	−4167
	$\text{CaMgSiO}_4$	−2329	−2360
	$\text{Mg}_2\text{SiO}_4$	−2283	−2299
	$\text{K}_{1.14}\text{Mg}_{0.57}(\text{Si}_{1.43}\text{O}_4)$	−2062	−2097
Phosphates	$\text{Ca}_2\text{KP}_3\text{O}_{10}$	−6794	−6935
	$\text{Mg}_2\text{P}_2\text{O}_7$	−4732	−4822
	$\text{KCaPO}_4$	−2665	−2723
	$\text{KMgPO}_4$	−2618	−2675
sulphates	$\text{K}_2\text{SO}_4$	−1188	−1245
	$\text{MgSO}_4$	−1334	−1376
	$\text{CaSO}_4$	−1381	−1425
<i>Values of <math>\Delta G</math> of the formation of exemplary simple silicates and phosphates</i>			
	$\text{CaSiO}_3$	−1679	−1701
	$\text{MgSiO}_3$	−1632	−1652
	$\text{K}_2\text{SiO}_3$	−1486	−1521
	$\text{Ca}_3(\text{PO}_4)_2$	−5523	−5626
	$\text{Mg}_3(\text{PO}_4)_2$	−5382	−5481
	$\text{K}_3\text{PO}_4$	−2472	−2544

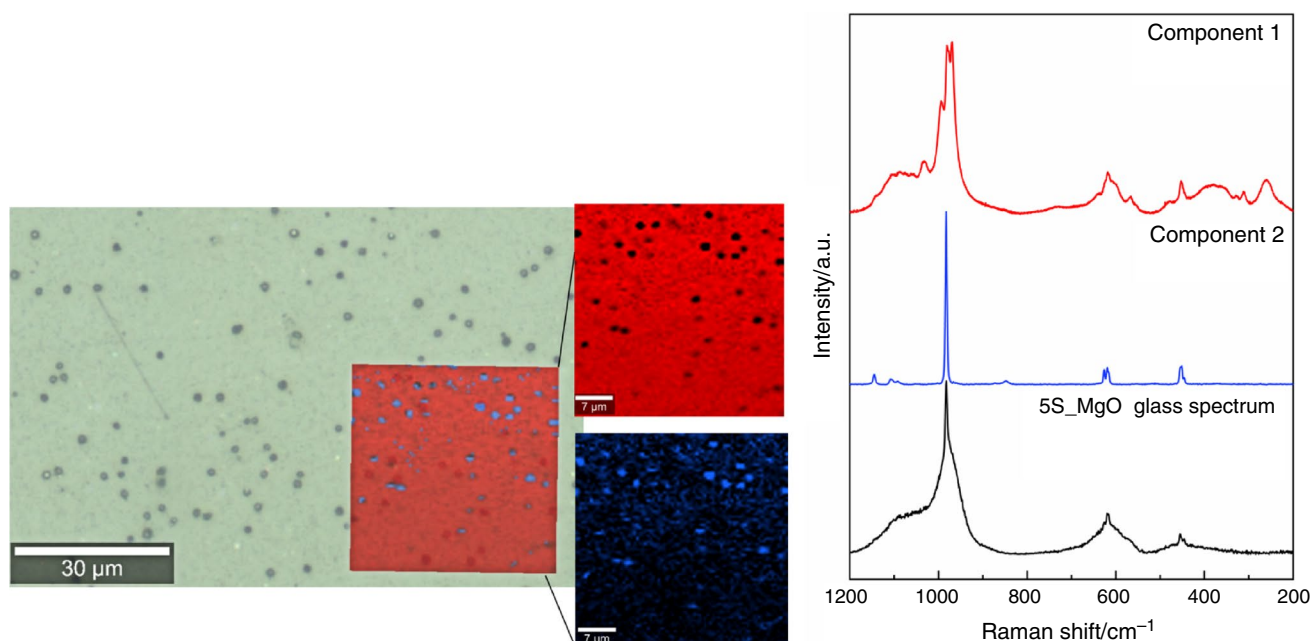


**Fig. 17** Raman maps of the surface fragment of 3S\_MgO devitrified sample (left) and Raman spectra taken at detected regions (right). Colours of the individual spectral lines correspond to those of surface regions, at which the data was collected

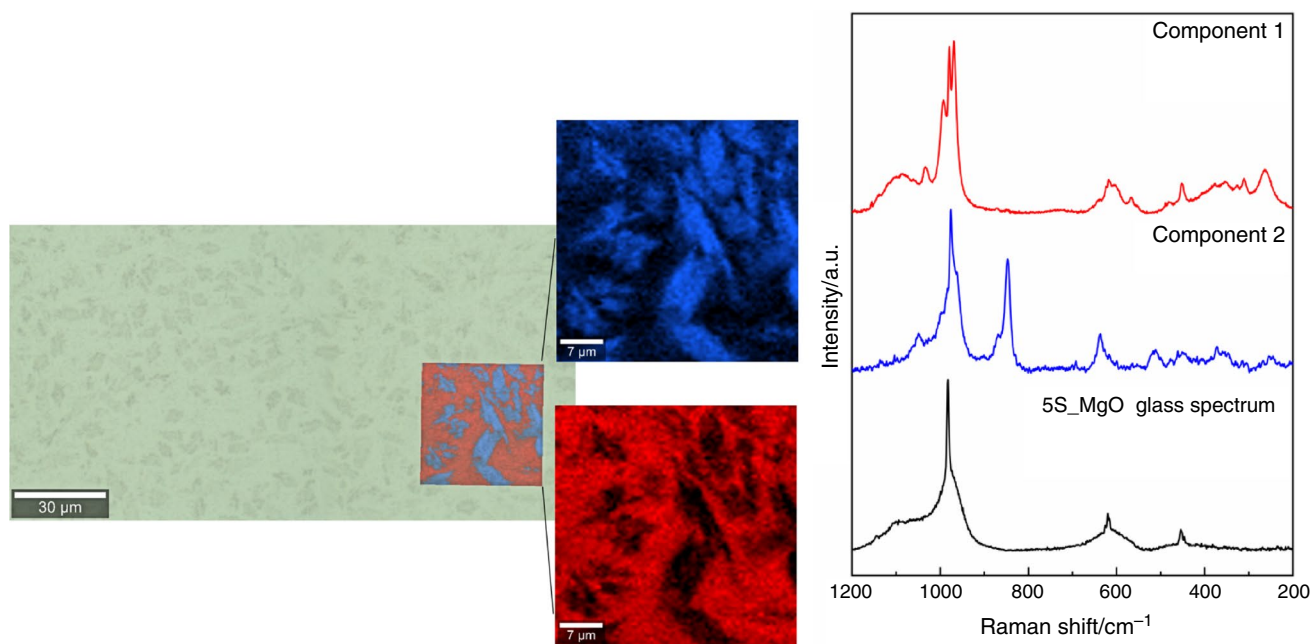


**Fig. 18** Raman maps of the surface fragment of 5S\_MgO devitrified sample (left) and Raman spectra taken at detected regions (right). Colours of the individual spectral lines correspond to those of surface regions, at which the data was collected

distinguish additional phase, predominantly consisting of crystalline  $K_2SO_4$  (which origin will be discussed in detail later in this section), while on the surface of 5S\_MgO sample elongated forms of the second phase (Component 2, blue spectrum) uniformly distributed within the dominant phase

(Component 1) appear, as shown in Fig. 18. Unfortunately, the complexity of the Raman spectrum of elongated crystallites, as well as the lack of suitable mineral standard spectrum in the database used impeded the proper identification of the detected component. Nonetheless, taking into account



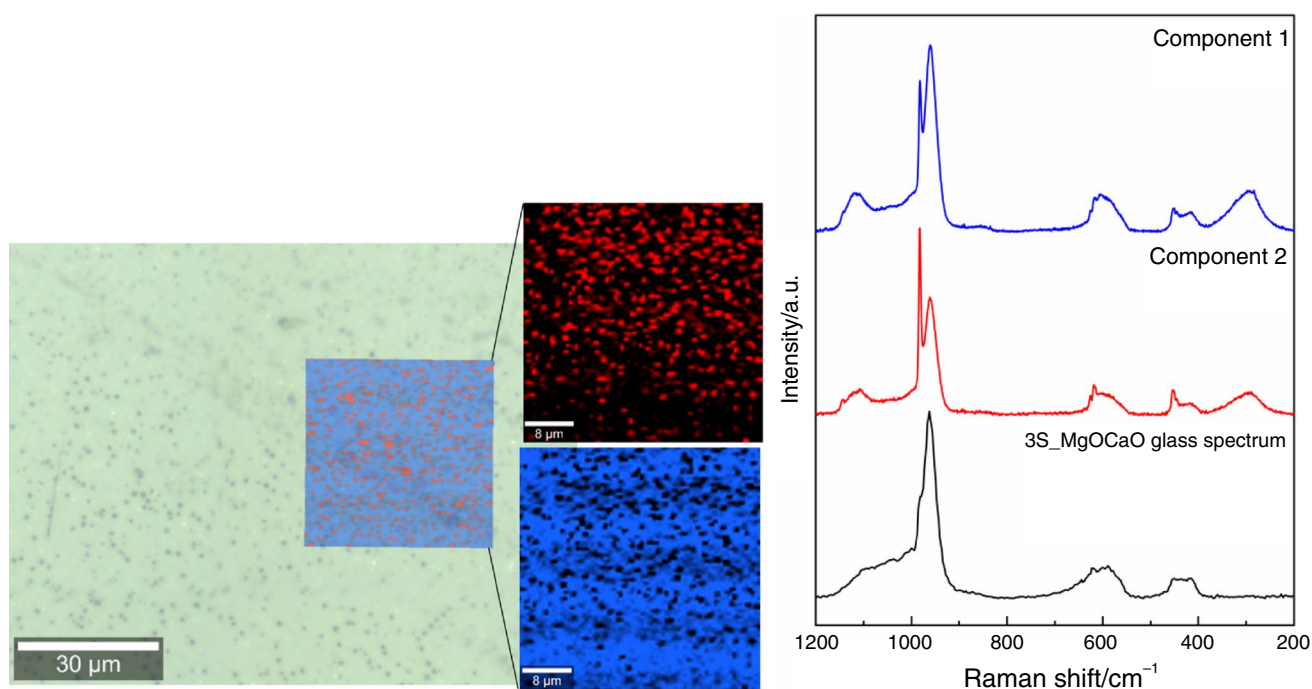


**Fig. 19** Raman maps of the surface fragment of 3S\_MgOCaO devitrified sample (left) and Raman spectra taken at detected regions (right). Colours of the individual spectral lines correspond to those of surface regions, at which the data was collected

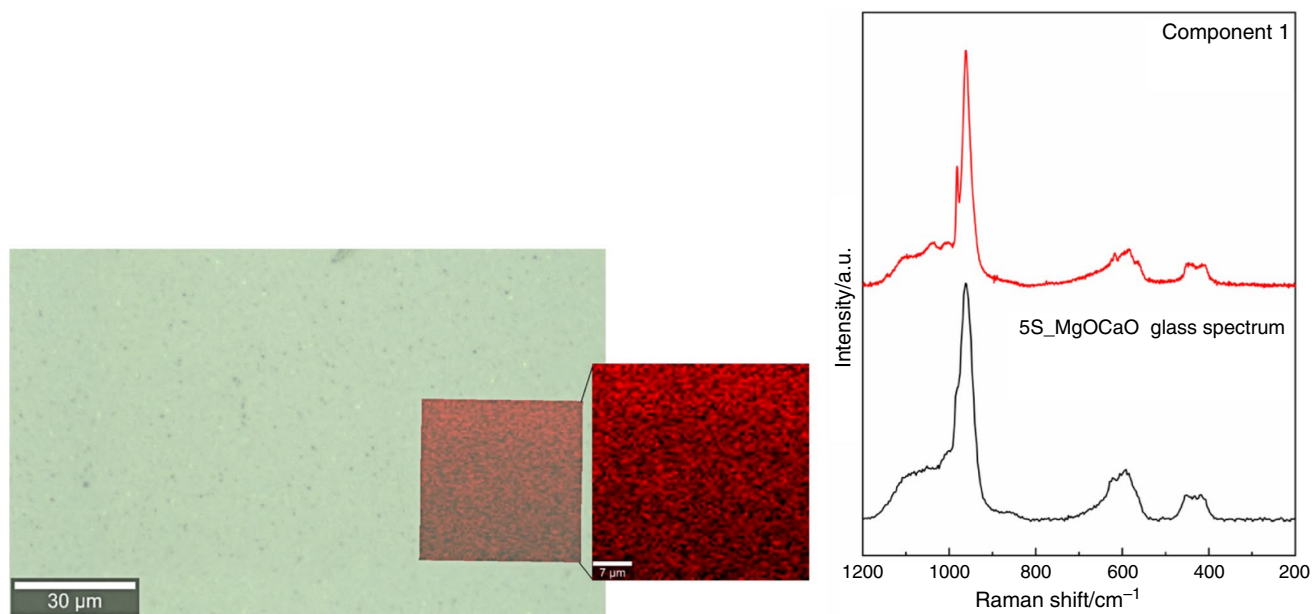


**Fig. 20** Raman maps of the surface fragment of 5S\_MgOCaO devitrified sample (left) and Raman spectra taken at detected regions (right). Colours of the individual spectral lines correspond to those of surface regions, at which the data was collected

the literature data as well as the experience from the previous study on those materials, it may be stated that this very phase has the structure of a complex silicate, since the most prominent bands of its spectrum, i.e. 975, 850, 640  $\text{cm}^{-1}$ , origin from stretching vibrations of  $\text{Si-O}^-$  terminal bonds

in  $\text{Q}^2$  units,  $\text{Q}^0$  units and  $\text{Si-O-Si}$  bridge vibrations, respectively [27, 50].

Meanwhile, the results obtained for the dual MgOCaO system (Figs. 19, 20) are much less intricate, which is surprising given the amount of crystalline phases detected

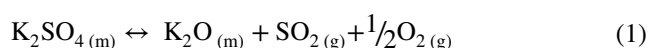
**Table 8** The assignment of characteristic vibrational bands from Raman spectra of sulphate-bearing multicomponent silicate-phosphate glasses

Frequency range/cm <sup>-1</sup>	Assignment
1200–850	Symmetric stretching vibrations of Si–O <sup>-</sup> terminal bonds in silicate units (the higher the number of non-bridging oxygens (NBOs) forming the SiO <sub>4</sub> tetrahedron, the lower is position of the band on the wavenumber scale)
700–500	Bending motions of Si–O–Si bridges in Q <sup>2*</sup> structural units, asymmetric bending vibrations of P–O <sup>-</sup> in orthophosphate groups (PO <sub>4</sub> ) <sup>3-</sup>
500–350	Bending vibrations of O–P–O and P–O <sup>-</sup> linkages in orthophosphate (PO <sub>4</sub> ) <sup>3-</sup> and pyrophosphate (P <sub>2</sub> O <sub>7</sub> ) <sup>4-</sup> units, respectively
Sulphate-specific Raman vibration modes	
1145	Asymmetric S–O stretching vibration, $\nu_{as}$ (S–O)
984	Symmetric S–O stretching vibration, $\nu_{ss}$ (S–O)
620	Asymmetric S–O–S bending vibration, $\delta_{as}$ (S–O–S)
455	Symmetric S–O–S bending vibration, $\delta_{ss}$ (S–O–S)

\*In Q<sup>n</sup> notation Q represents silicate (or phosphate) tetrahedron, while n is the number of bridging oxygens (BOs) in a given unit

in respective devitrificates by the XRD method (see Sect. 3.2.1). As regards the 3S\_MgOCaO sample, the presence of two different regions has been revealed on the studied profile (Fig. 19), while only one component apparently constitutes the bulk of the 5S\_MgOCaO sample. Interestingly, all the Raman spectra taken at the detected regions have analogous character, which additionally corresponds to the respective spectra of the initial glasses. The only sharp and well-defined peaks (1145, 982, 618, 453 cm<sup>-1</sup>) superimposed on the relatively broad spectral lines specific for residual amorphous phase may be ascribed to K<sub>2</sub>SO<sub>4</sub> phase. Judging by the relative intensities of sulphate-related peaks as regards 3S\_MgOCaO sample it is clear that the Component 2 (red) has considerably higher content of as-identified compound than the Component 1, which constitutes the majority of this very material (Fig. 19). Finally, it should be mentioned that the narrower character of spectral lines in the 5S\_MgOCaO sample's Raman spectrum (Fig. 20) implies the increased amount of crystalline phase compared to the one containing 3 mol.% of sulphate.

Unexpectedly, the Raman imaging method has also shed some light on the mechanism of sulphate incorporation into the glassy matrix. It may be clearly seen (especially on the analysed profiles of the 3S samples, while on those of the 5S samples only after close examination) that the studied fragments are covered with the remnants of gas bubbles (visible e.g. in Figs. 17, 19). Interestingly, precisely those very regions are marked by particularly high content of sulphate, which is manifested by the respective Raman spectra (Fig. 17: Component 2, blue spectrum; Fig. 19: Component 2, red spectrum). It is common in the glass technology to use sulphates as fining agents, which serve as a source of gas, clarifying the melt [51]. Such sulphates, when present in a melt, readily dissolve into its alkali-rich regions and then, at sufficiently high temperatures (~ 1200 °C for K<sub>2</sub>SO<sub>4</sub> [52]) decompose (under oxidizing conditions) according to the reaction (based on the Ref. [53]):



As the solubility of sulphates is known to be low in the silicate-rich melts only a certain part of the resulting SO<sub>2</sub> may be dissolved in the melt and occupies the 'solubility sites' (which are the voids of the glass network [5, 54]) forming the sulphate domains in a close surrounding of a alkali metal cations. A clear demonstration of such phenomenon constitute Raman spectra of Component 1 and Component in the Figs. 17 and 19, respectively, on which, among the features corresponding to the main phase, also the bands specific for [SO<sub>4</sub>]<sup>2-</sup> anion vibrations emerge. Meanwhile, the other part of SO<sub>2</sub> formed as a result of the reaction (1) is liberated in the form of gas and forms bubbles. And precisely remnants of those are believed to mark their presence on the profiles of studied samples (Figs. 17, 19). Worth attention are also the regions of analysed surfaces surrounding the bubbles' residues. As the [SO<sub>4</sub>]<sup>2-</sup>-specific bands are prominent on the Raman spectra taken at those peculiar areas it is reasonable to state, that they are markedly enriched with sulphate. A possible explanation for such observation lies in the fact that lowering the temperature after pouring the melt may result in reabsorption of some of SO<sub>2</sub> from bubbles to form regions especially enriched with sulphate [55].

It is also important to mention here the noticeable differences between the outcomes of XRD (see Sect. 3.2.1) and RSI phase identification, for which several factors may be held responsible. As the first different detection thresholds of both the methods used should be pointed out. Of utter importance is also deemed to be the form of the devitrified samples submitted to analysis, since while for the XRD analysis the 0.1–0.3 mm fraction has been used, much larger piece of material were analysed by the Raman imaging spectroscopy technique. Therefore, in all likelihood, predominantly surface crystallization has been induced during devitrification process of the latter. In addition to the above, also the microsection preparation is not without significance, as

it results in a removal of the top layer of a sample given that it may be stated that detection of lower number of crystalline phases as regards the RSI microsection analysis is justifiable and it was the employment of both the above-mentioned techniques that provided a complete overview of the domain structure of studied materials.

## Conclusions

The present study was motivated by the need to develop materials capable of supplying plants with bioavailable sulphur by synthesizing and thoroughly investigating three different glass systems:  $\text{SiO}_2\text{--P}_2\text{O}_5\text{--K}_2\text{O--MgO--SO}_3$  (the MgO series),  $\text{SiO}_2\text{--P}_2\text{O}_5\text{--K}_2\text{O--CaO--SO}_3$  (the CaO series) and  $\text{SiO}_2\text{--P}_2\text{O}_5\text{--K}_2\text{O--MgO--CaO--SO}_3$  (the MgOCaO series).

Years of studying the structure and properties of sulphate-bearing glasses have proven that enclosing the  $\text{SO}_4^{2-}$  ions in the amorphous matrix is a complex and delicate matter, highly influenced by a set of factors. And although obtaining sulphate-bearing glasses is in fact challenging itself, development of such materials but intended for plant fertilization places additional requirements on the final product, which are as follows:

1. Amorphicity of the synthesized materials was verified by means of XRD analysis, results of which indicated that the MgO system was the only one represented by fully amorphous samples (within the range of 0–3 mol.% of  $\text{SO}_3$ ), while all the materials from remaining series (XS\_CaO, XS\_MgOCaO) displayed a tendency toward devitrification during cooling the melt.
2. Adequate content of components having nutritional value for plants, with emphasis on sulphate content (i.e. sulphate capacity of glasses)—was established by combination of XRF method as well as semiquantitative SEM–EDS analysis. It was showed that samples representing both the CaO and MgOCaO systems are characterized by low sulphate capacity (~0.9 mol.% of  $\text{SO}_3$  introduced, i.e. 1 mol.% of  $\text{SO}_3$  nominal, before crystallization of  $\text{K}_2\text{SO}_4$  takes place) in relation to the MgO system, in the structure of which as much as 2 mol.% of sulphate (i.e. 3 mol.% nominal) was enclosed. Furthermore, basing on the observed discrepancies between the XRF- and SEM–EDS-determined  $\text{SO}_3$  amounts, it was suggested that  $\text{K}_2\text{SO}_4$  formed as a result of an exceeded sulphate capacity of glasses is non-uniformly distributed (presumably in the surface area) within the volume of obtained materials.
3. Capability of the acquired materials to remove the components from the structure to the soil environment—preliminary assessment of which may be founded on the study of thermal stability of samples and their ability to crystallize, as it is known that the higher ability of the fertilizing glasses for crystallization the higher their ability to release the nutrients present the glassy framework. Results of the comprehensive thermal analysis involving DSC method supplemented with the calculations of glass stability (GS) parameters:
  - Eliminated the CaO series from further studies, as no glass-specific thermal effects were noted on the respective DSC curves;
  - Demonstrated that in both the MgO- and the MgOCaO-containing systems the  $\text{SO}_3$  additive increases the values of  $T_g$  and decreases the vitreous state transformation range, compared to the input materials. Such result may constitute a manifestation of polymerizing effect of  $\text{SO}_4^{2-}$  ions on the silicate subnetwork as well as of the progressive increase in the structure rigidity along with the sulphate content;
  - Illustrated that an increase in sulphate content in the amorphous representants of the MgO series (0–3 mol.% of  $\text{SO}_3$  addition) results in a subsequent decrease in their thermal stability, while for the semicrystalline samples (5S\_MgO, XS\_MgOCaO) the tendency is opposite, owing to the superior stability of such materials compared to the fully amorphous ones.
4. The character of domain structure, which determines the chemical activity of glassy fertilizers in biological solutions, as well as the distribution of such groupings, was investigated on the samples submitted to devitrification process (MgO, MgOCaO series), by means of two techniques giving complementary results, i.e. XRD and Raman imaging spectroscopy (RSI). It was found that in the structure of studied samples there are present three types of domains:
  - Various groupings based on silicate units, constituting the major phase of the studied materials;
  - The groupings of the orthophosphate type, mainly  $\text{KMgPO}_4$  as regards the MgO series and  $\text{KCaPO}_4$  in the case of the dual one, distributed in the volume of dominant, silicate phase;
  - sulphate-containing  $\text{K}_2\text{SO}_4$  phase, present either as groupings distributed within the dominant (presumably in the voids of) silicate phase, or surrounding the remnants of the gas bubbles.

The above presented findings prove the utter importance of the glass composition in the designing process of sulphate-bearing glasses, as even seemingly negligible

change in the form of introducing different alkaline earth network modifiers species has a significant impact on the glass behaviour from the point of view of  $\text{SO}_3$  incorporation. Furthermore, it turns out that obtaining amorphous materials in such systems is a complicate manoeuvre between attaining suitable polymerization degree of the melt, low enough to facilitate incorporation of sulphate species, and maintaining melt's high viscosity in order to surpass its spontaneous devitrification during cooling. And although the obtained and presented in this work results indicate unambiguously that the most promising matrix for enclosing sulphate species is the  $\text{MgO}$ -containing composition, as the remaining systems displayed the tendency towards reorganization into the stable compounds, further studies are planned to amorphisize materials representing the prone-to-crystallization series by means of increasing the rate of cooling the respective melts.

**Acknowledgements** The authors would like to express their sincere gratitude for the XRD to DSc. Bartosz Handke, (Faculty of Materials Science and Ceramics, AGH University of Science and Technology in Krakow, Poland). The authors also gratefully acknowledge the invaluable help of Prof. Konrad Świerczek (Faculty of Energy and Fuels, AGH University of Science and Technology in Krakow, Poland) in performing the HT-XRD experiment. This work was financed by the National Science Centre, Poland, project number 2018/31/D/ST8/03148.

**Authors' contribution** The first draft of the present manuscript was written by Anna Berezicka, while Magdalena Szumera and Justyna Sułowska provided critical feedback and commented on the previous versions of manuscript. Anna Berezicka synthesized materials, collected the data, analysed and interpreted them. Piotr Jeleń performed the Raman Imaging technique, while Radosław Lach characterized the samples with XRD method. All authors discussed the results, helped shape the research as well as read and approved the final manuscript.

**Open Access** This article is licensed under a Creative Commons Attribution 4.0 International License, which permits use, sharing, adaptation, distribution and reproduction in any medium or format, as long as you give appropriate credit to the original author(s) and the source, provide a link to the Creative Commons licence, and indicate if changes were made. The images or other third party material in this article are included in the article's Creative Commons licence, unless indicated otherwise in a credit line to the material. If material is not included in the article's Creative Commons licence and your intended use is not permitted by statutory regulation or exceeds the permitted use, you will need to obtain permission directly from the copyright holder. To view a copy of this licence, visit <http://creativecommons.org/licenses/by/4.0/>.

## References

- Nascimento MLF, Souza LA, Ferreira EB, Zanotto ED. Can glass stability parameters infer glass forming ability? *J Non Cryst Solids*. 2005;351:3296–308.
- Stoch L. Structure and crystallization of multicomponent glasses. *High Temp Mater Process*. 1992;10:245–64.
- Ooura M, Hanada T. Compositional dependence of solubility of sulphate in silicate glasses. *Glas Technol*. 1998;39:68–73.
- Jantzen CM, Smith ME, Peeler DK. Dependency of sulfate solubility on melt composition and melt polymerization. *Ceram Trans*. 2005;168:141–52.
- Manara D, Grandjean A, Pinet O, Dussossoy JL, Neuville DR. Sulfur behavior in silicate glasses and melts: Implications for sulfate incorporation in nuclear waste glasses as a function of alkali cation and  $\text{V}_2\text{O}_5$  content. *J Non Cryst Solids*. 2007;353:12–23.
- Manara D, Grandjean A, Pinet O, Dussossoy JL, Neuville DR. Factors influencing the sulphate incorporation in radioactive waste glasses. *Mater Res Soc Symp Proc*. 2006. <https://doi.org/10.1557/PROC-932-84.1>.
- Förland T, Weyl WA. Formation of a sulfate glass. *J Am Ceram Soc*. 1950;33:186–8.
- Waclawska I, Stoch L. Thermal behaviour of silicate-phosphate glasses in relation to their biochemical activity. *J Therm Anal Calorim*. 2021;65:141–6.
- Stoch L, Waclawska I, Ciecina M. Thermochemistry of biologically active glasses. *J Therm Anal Calorim*. 2001;65(2):341–50. <https://doi.org/10.1023/A:1017948212869>.
- Waclawska I, Szumera M, Stoch P, Sitarz M. Structural role of Fe in the soil active glasses. *Spectrochim Acta Part A Mol Biomol Spectrosc*. 2011;79(4):728–32. <https://doi.org/10.1016/j.saa.2010.08.045>.
- Kilpeläinen T, Pajula K, Ervasti T, Uurasjärvi E, Koistinen A, Korhonen O. Raman imaging of amorphous-amorphous phase separation in small molecule co-amorphous systems. *Eur J Pharm Biopharm*. 2020;155:49–54. <https://doi.org/10.1016/j.ejpb.2020.08.007>.
- Sitarz M, Bulat K, Wajda A, Szumera M. Direct crystallization of silicate-phosphate glasses of  $\text{NaCaPO}_4\text{-SiO}_2$  system. *J Therm Anal Calorim*. 2013. <https://doi.org/10.1007/s10973-013-3240-y>.
- Sitarz M, Bulat K, Szumera M. Influence of modifiers and glass-forming ions on the crystallization of glasses of the  $\text{NaCaPO}_4\text{-SiO}_2$  system. *J Therm Anal Calorim*. 2012;109(2):577–84. <https://doi.org/10.1007/s10973-011-2156-7>.
- Erasmus EP, Sule R, Johnson OT, Massera J, Sigalas I. In vitro evaluation of porous borosilicate, borophosphate and phosphate bioactive glasses scaffolds fabricated using foaming agent for bone regeneration. *Sci Rep*. 2018. <https://doi.org/10.1038/s41598-018-22032-2>.
- Ojovan MI, Lee WE, Kalmykov SN. An introduction to nuclear waste immobilisation. Elsevier; 2019.
- Mishra RK, Sudarsan KV, Sengupta P, Vatsa RK, Tyagi AK, Kaushik CP, et al. Role of sulfate in structural modifications of sodium barium borosilicate glasses developed for nuclear waste immobilization. *J Am Ceram Soc*. 2008;91:3903–7.
- Kaushik CP, Mishra RK, Sengupta P, Kumar A, Das D, Kale GB, et al. Barium borosilicate glass—a potential matrix for immobilization of sulfate bearing high-level radioactive liquid waste. *J Nucl Mater*. 2006;358:129–38. <https://doi.org/10.1016/j.jnucmat.2006.07.004>.
- Stefanovsky SV, Stefanovsky OI, Prusakov IL, Kadyko MI, Averin AA, Nikonov BS. Speciation of sulphate ions in sodium alumino(iron)phosphate glasses. *J Non Cryst Solids*. 2019;512:81–9. <https://doi.org/10.1016/j.jnoncrysol.2019.01.005>.
- Morizet Y, Ory S, Di Carlo I, Scaillet B, Echegut P. The effect of sulphur on the glass transition temperature in anorthite-diopside eutectic glasses. *Chem Geol*. 2015. <https://doi.org/10.1016/j.chemgeo.2015.10.010>.
- Wang X, Wu L, Li H, Xiao J, Cai X, Teng Y. Preparation and characterization of  $\text{SO}_3$ -doped barium borosilicate glass-ceramics containing zirconolite and barite phases. *Ceram Int*. 2017. <https://doi.org/10.1016/j.ceramint.2016.09.190>.
- Loneragan JM, Lonergan C, Silverstein J, Cholsaipant P, McCloy J. Thermal properties of sodium borosilicate glasses as a function of sulfur content. *J Am Ceram Soc*. 2020;103:3610–9.



22. Hrubý A. Evaluation of glass-forming tendency by means of DTA. *Czechoslov J Phys.* 1972;22:1187–93.
23. Turnbull D. Under what conditions can a glass be formed? *Contemp Phys.* 1969;10:473–88.
24. Lu ZP, Liu CT. A new glass-forming ability criterion for bulk metallic glasses. *Acta Mater.* 2002;50(13):3501–12. [https://doi.org/10.1016/S1359-6454\(02\)00166-0](https://doi.org/10.1016/S1359-6454(02)00166-0).
25. Vienna JD, Kim DS, Muller IS, Piepel GF, Kruger AA. Toward understanding the effect of low-activity waste glass composition on sulfur solubility. *J Am Ceram Soc.* 2014;97:3135–42.
26. Stoch L. Thermal analysis and thermochemistry of vitreous into crystalline state transition. *J Therm Anal Calorim.* 2004;77(1):7–16. <https://doi.org/10.1023/B:JTAN.0000033182.90571.ce>.
27. Berezicka A, Szumera M, Sułowska J, Jeleń P, Olejniczak Z, Stepień J, et al. Unraveling the nature of sulfur-bearing silicate-phosphate glasses: insights from multi-spectroscopic (Raman, MIR, <sup>29</sup>Si, <sup>31</sup>P MAS-NMR, XAS, XANES) investigation. *Ceram Int.* 2022. <https://doi.org/10.1016/j.ceramint.2021.10.216>.
28. Wacławska I, Środa M, Stoch L. Thermal methods applied to the glass transition of mixed network AlPO<sub>4</sub>-BPO<sub>4</sub>-SiO<sub>2</sub> glasses. *J Therm Anal Calorim.* 2001;65:661–7.
29. Stoch L. Flexibility of structure as a criterion of glass formation and stability. *Opt Appl.* 2000;30:647–55.
30. Stoch P, Ciecinska M, Stoch A. Thermal properties of phosphate glasses for salt waste immobilization. *J Therm Anal Calorim.* 2014;117(1):197–204. <https://doi.org/10.1007/s10973-014-3698-2>.
31. Testasica LP, Frost RL, Ruan X, Lima J, Belotti FM, Scholz R. The application of high-temperature X-ray diffraction and infrared emission spectroscopy to the thermal decomposition of kröhnkite. *J Therm Anal Calorim.* 2016;126:1089–95.
32. Avramov I, Zanutto ED, Prado MO. Glass-forming ability versus stability of silicate glasses. II. Theoretical demonstration. *J Non Cryst Solids.* 2003;320(1–3):9–20. [https://doi.org/10.1016/S0022-3093\(03\)00081-4](https://doi.org/10.1016/S0022-3093(03)00081-4).
33. Zanutto ED. Isothermal and adiabatic nucleation in glass. *J Non Cryst Solids.* 1987;89:361–70.
34. Goj P, Ciecinska M, Szumera M, Stoch P. Thermal properties of Na<sub>2</sub>O–P<sub>2</sub>O<sub>5</sub>–Fe<sub>2</sub>O<sub>3</sub> polyphosphate glasses. *J Therm Anal Calorim.* 2020;142(1):203–9. <https://doi.org/10.1007/s10973-020-09476-3>.
35. Kozmidis-Petrovic A, Šesták J. Forty years of the Hrubý glass-forming coefficient via DTA when comparing other criteria in relation to the glass stability and vitrification ability. *J Therm Anal Calorim.* 2011;110(2):997–1004. <https://doi.org/10.1007/s10973-011-1926-6>.
36. Jha P, Singh K. Effect of MgO on bioactivity, hardness, structural and optical properties of SiO<sub>2</sub>–K<sub>2</sub>O–CaO–MgO glasses. *Ceram Int.* 2016;42(1):436–44. <https://doi.org/10.1016/j.ceramint.2015.08.128>.
37. Jha P, Danewalia SS, Singh K. Influence of thermal stability on dielectric properties of SiO<sub>2</sub>–K<sub>2</sub>O–CaO–MgO glasses. *J Therm Anal Calorim.* 2017;128:745–54.
38. Wacławska I, Szumera M. Influence of MgO (CaO) on the structure of silicate-phosphate glasses: TA and NMR study. *J Therm Anal Calorim.* 2006;84(1):185–90. <https://doi.org/10.1007/s10973-005-7183-9>.
39. Watts SJ, Hill RG, O'Donnell MD, Law RV. Influence of magnesia on the structure and properties of bioactive glasses. *J Non Cryst Solids.* 2010;356:517–24.
40. Wacławska I, Szumera M. Thermal behaviour of Fe-doped silicate–phosphate glasses. *J Therm Anal Calorim.* 2010;101(2):423–7. <https://doi.org/10.1007/s10973-010-0798-5>.
41. Sitarz M, Szumera M. Crystallization of silico-phosphate glasses. *J Therm Anal Calorim.* 2007;91(1):255–60. <https://doi.org/10.1007/s10973-007-8374-3>.
42. Wacławska I, Szumera M. Spectroscopic and thermal studies of silicate-phosphate glass. *J Therm Anal Calorim.* 2007;88(1):151–6. <https://doi.org/10.1007/s10973-006-8118-9>.
43. Wacławska I, Szumera M. Thermal analysis of glasses for proecological applications. *J Therm Anal Calorim.* 2003;72(3):1065–72. <https://doi.org/10.1023/A:1025059424522>.
44. Wacławska I, Szumera M. Effect of molybdenum addition on the thermal properties of silicate–phosphate glasses. *J Therm Anal Calorim.* 2012;109(2):649–55. <https://doi.org/10.1007/s10973-012-2399-y>.
45. Stoch L. Flexibility of structure and glass-forming ability: a chemical approach. *Glas Phys Chem.* 2001;27:167–74.
46. Barin I. *Thermochemical data of pure substances.* Wiley-VCH Verlag GmbH; 1995.
47. Miladi L, Oueslati A, Guidara K. Vibrational spectroscopic and dielectric properties investigations of phase transitions in KMgPO<sub>4</sub> compound. *J Mol Struct.* 1979;1148: 404–11.
48. Miladi L, Oueslati A, Guidara K. Phase transition, conduction mechanism and modulus study of KMgPO<sub>4</sub> compound. *RSC Adv R S Chem.* 2016;6:83280–7.
49. McKeown DA, Muller IS, Gan H, Pegg IL, Kendziora CA. Raman studies of sulfur in borosilicate waste glasses: sulfate environments. *J Non Cryst Solids.* 2001;288(1–3):191–9. [https://doi.org/10.1016/S0022-3093\(01\)00624-X](https://doi.org/10.1016/S0022-3093(01)00624-X).
50. McMillan P. A Raman spectroscopic study of glasses in the system CaO–MgO–SiO<sub>2</sub>. *Am Mineral.* 1984;69:645–59.
51. Mills HN. Use of fining agents. In: Smothers WJ, editor. *Proceedings of the 46th conference on glass problems: ceramic engineering and science proceedings*; 1986. p. 404–9.
52. Wang Z, Yang W, Liu H, Jin H, Chen H, Su K, et al. Thermochemical behavior of three sulfates (CaSO<sub>4</sub>, K<sub>2</sub>SO<sub>4</sub> and Na<sub>2</sub>SO<sub>4</sub>) blended with cement raw materials (CaO–SiO<sub>2</sub>–Al<sub>2</sub>O<sub>3</sub>–Fe<sub>2</sub>O<sub>3</sub>) at high temperature. *J Anal Appl Pyrolysis.* 2019;142:104617.
53. Pilon L. Foams in glass manufacturing. In: Stevenson P, editor. *Foam engineering: fundamentals and applications.* Wiley; 2012. p. 355–409. <https://doi.org/10.1002/9781119954620.ch16>.
54. Brendebach B, Denecke MA, Roth G, Weisenburger S. Sulfur incorporation in high level nuclear waste glass: A S K-edge XAFS investigation. *J Phys Conf Ser.* 2009;190:012186. <https://doi.org/10.1088/1742-6596/190/1/012186>.
55. Shelby JE. *Introduction to glass science and technology.* 2nd ed. Hilos Tensados; 2005. p. 45.

**Publisher's Note** Springer Nature remains neutral with regard to jurisdictional claims in published maps and institutional affiliations.